Supporting information

Edge-doped substituents as an emerging atomic-level strategy for enhancing M-N_4-C single-atom catalysts in electrocatalysis of ORR, OER, and HER

Liang Xie[a], Wei Zhou[a*], Zhibin Qu[a], Yuming Huang[a], Longhao Li[a], Chaowei Yang[a], Junfeng Li[a], Xiaoxiao Meng[a], Fei Sun[a], Jihui Gao[a], Guangbo Zhao[a].

a School of Energy Science and Engineering, Harbin Institute of Technology, Harbin, Heilongjiang, 150001 P. R. China

* Corresponding author:

E-mail addresses: hitzhouw@hit.edu.cn (Wei Zhou)

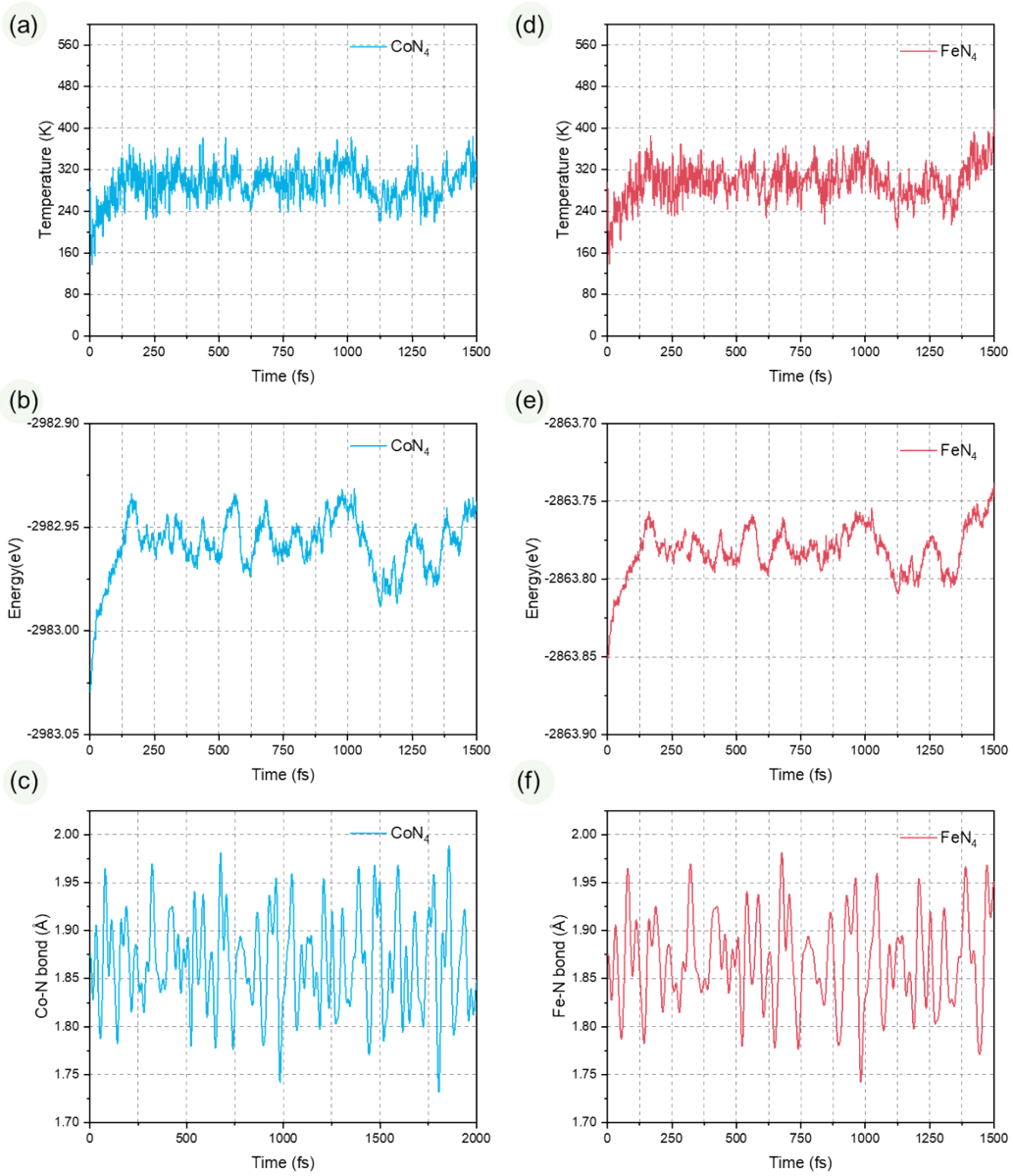

Figure S1. The variations of (a) temperature, (b) energy and (c) Co-N bond versus the AIMD simulation time for 1500fs of CoN_4 under 298.15 K. The variations of (d) temperature, (e) energy and (f) Fe-N bond versus the AIMD simulation time for 1500fs of FeN_4 under 298.15 K. Ab initio molecular dynamics calculations at the B97-3c level [1] using ORCA program [2-4] structural relaxation was performed at 298.15K

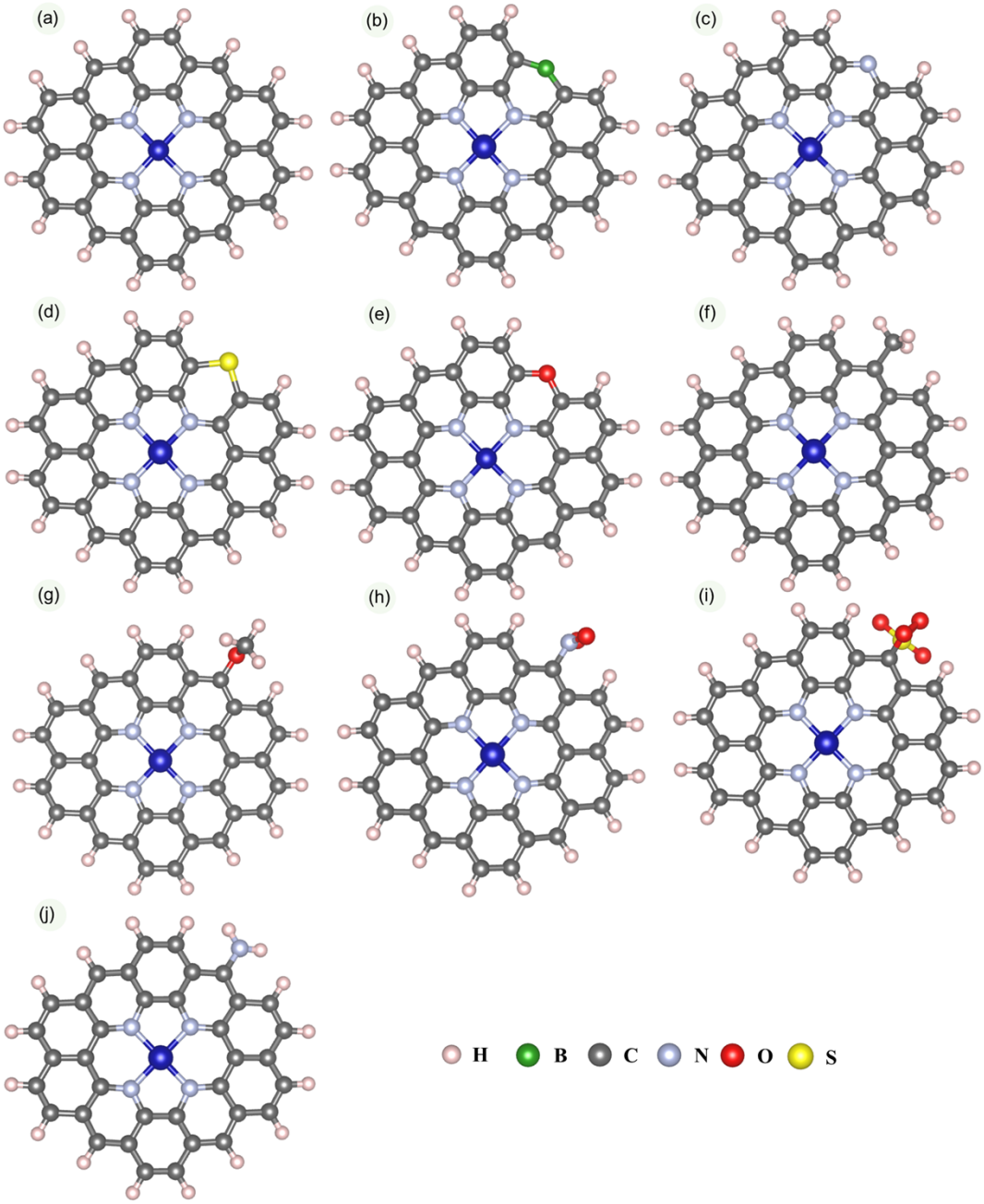

Figure S2. Optimized structure of Sub@FeN_4. (a) FeN_4 , (b) B@FeN_4 , (c) N@FeN_4 , (d) S@FeN_4 , (e) O@FeN_4 , (f) CH_3@FeN_4 , (g) OCH_3@FeN_4 , (h) NO_2@FeN_4 , (i) SO_4@FeN_4 , (j) NH_2@FeN_4.

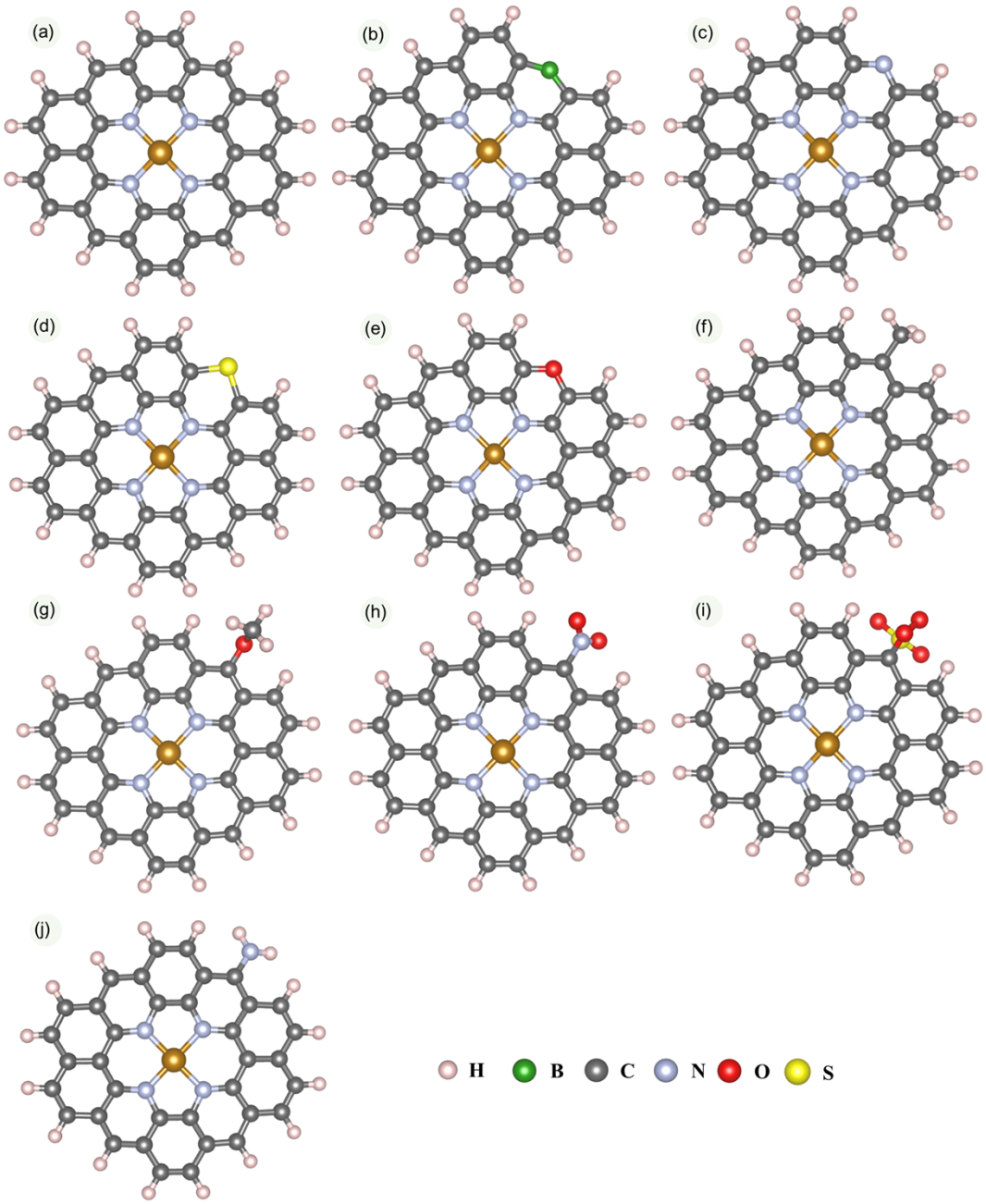

Figure S3. Optimized structure of Sub@CoN_4. (a) CoN_4 , (b) B@CoN_4 , (c) N@CoN_4 , (d) S@CoN_4 , (e) O@CoN_4 , (f) CH_3@CoN_4 , (g) OCH_3@CoN_4 , (h) NO_2@CoN_4 , (i) SO_4@CoN_4 , (j) NH_2@CoN_4.

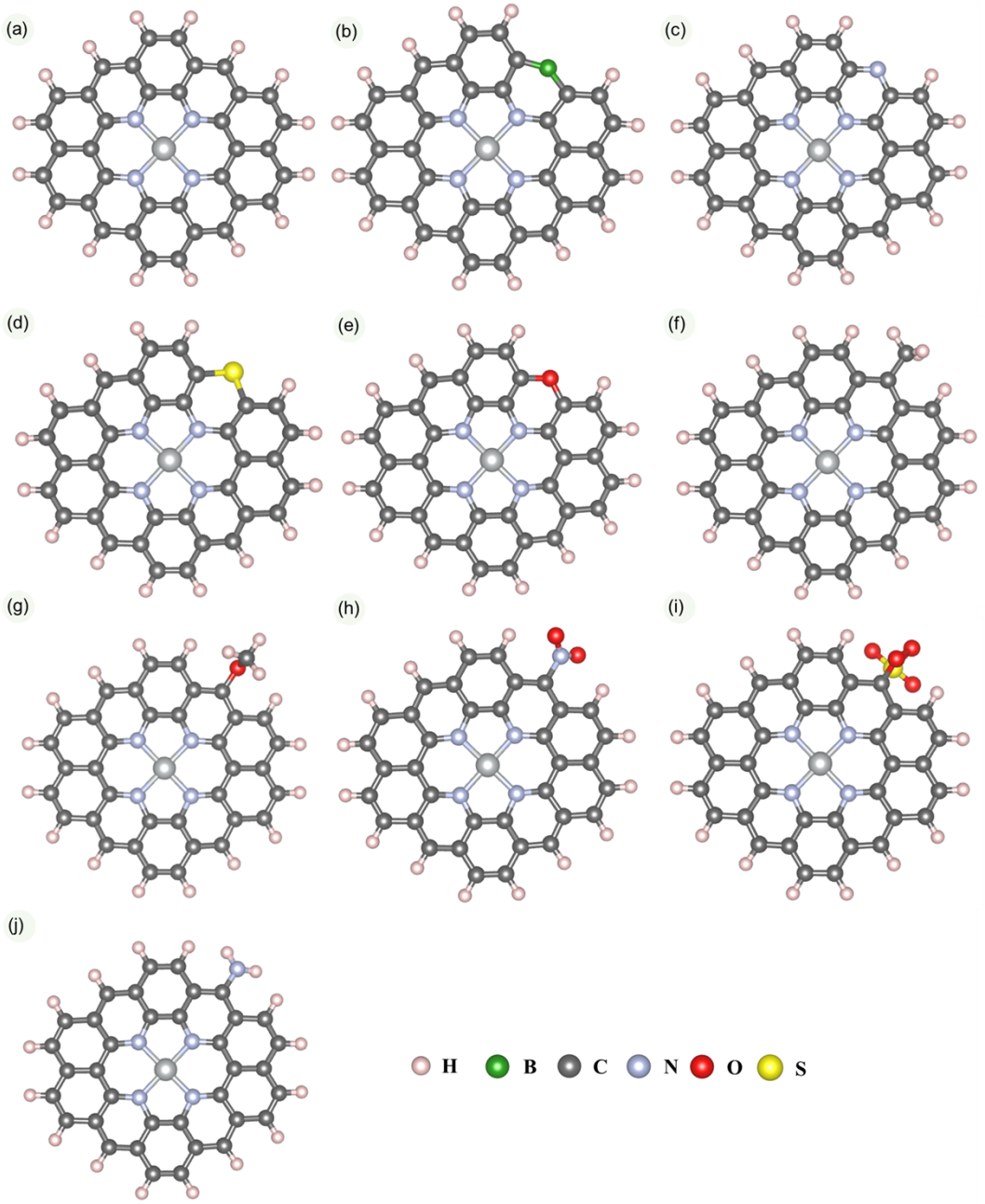

Figure S4. Optimized structure of Sub@NiN_4. (a) NiN_4 , (b) B@NiN_4 , (c) N@NiN_4 , (d) S@NiN_4 , (e) O@NiN_4 , (f) CH_3@NiN_4 , (g) OCH_3@NiN_4 , (h) NO_2@NiN_4 , (i) SO_4@NiN_4 , (j) NH_2@NiN_4.

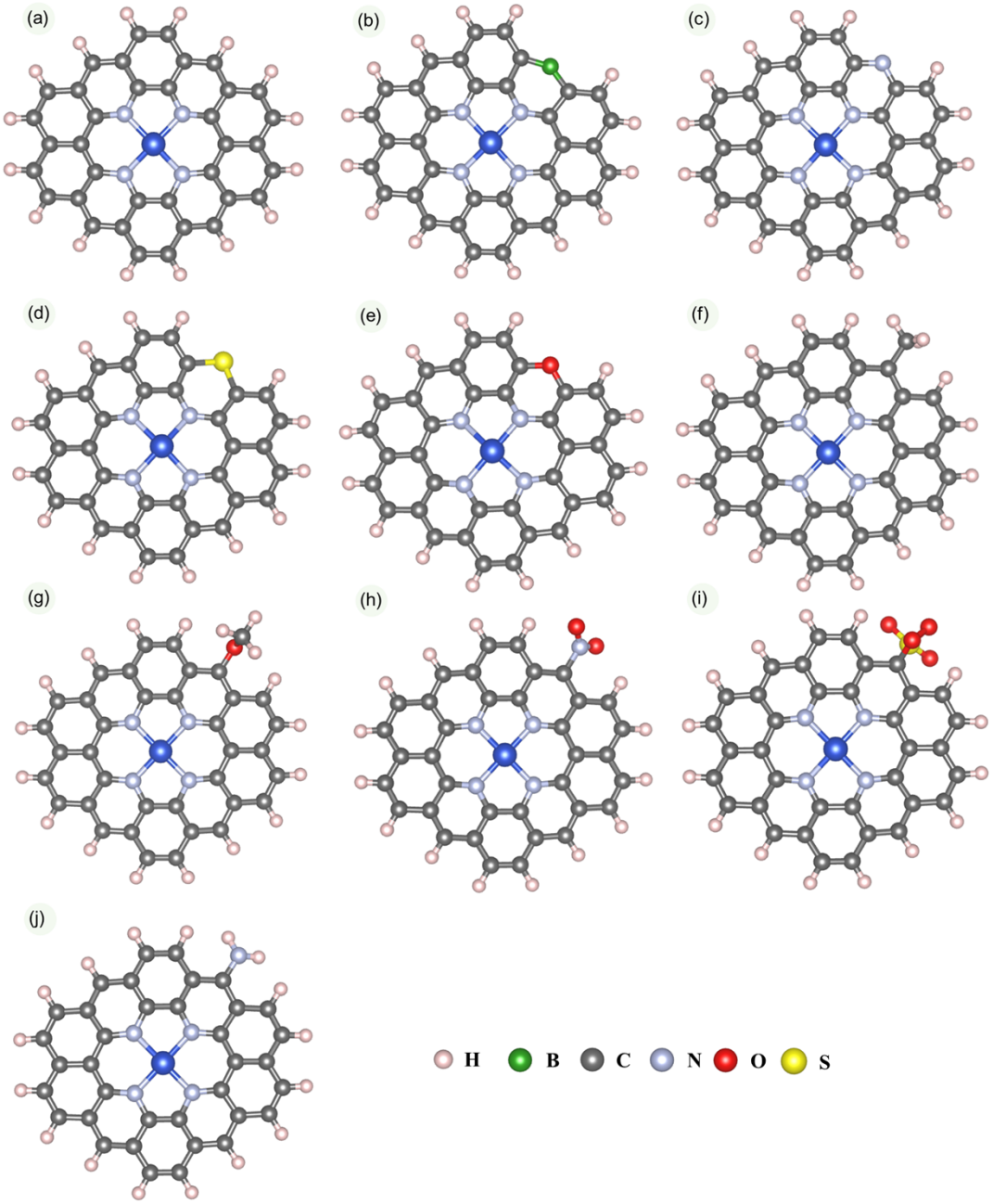

Figure S5. Optimized structure of Sub@CuN_4. (a) CuN_4 , (b) B@CuN_4 , (c) N@CuN_4 , (d) S@CuN_4 , (e) O@CuN_4 , (f) CH_3@CuN_4 , (g) OCH_3@CuN_4 , (h) NO_2@CuN_4 , (i) SO_4@CuN_4 , (j) NH_2@CuN_4.

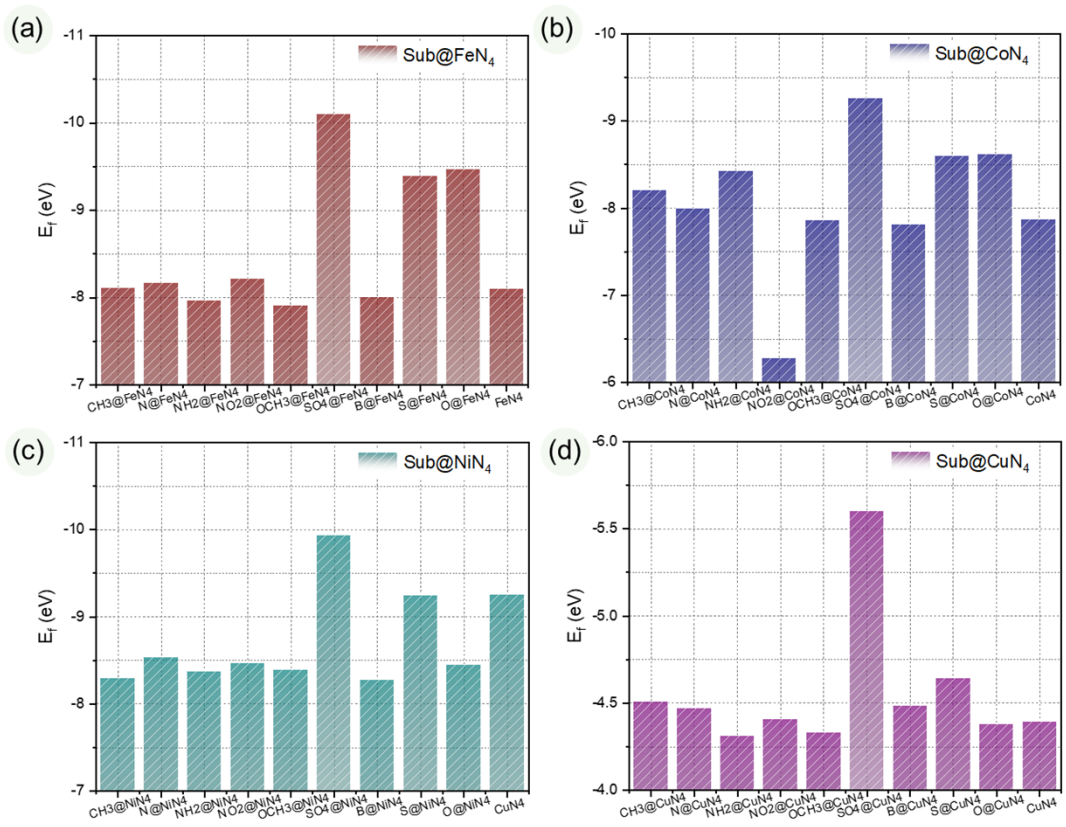

Figure S6 The formation energy of Sub@MN_4. (a) Sub@FeN_4; (b) Sub@CoN_4; (c) Sub@NiN_4; (d) Sub@CuN_4. The formula for calculating the formation energy is as follows: $E_f = E_{Sub@MN_4} - E_{Sub@N_4} - E_M$. In theoretical calculations, this indicator is widely used to assess stability, where $E_{Sub@MN_4}$, $E_{sub@N_4}$ and E_M represent the electronic energies of Sub@MN_4, Sub@N_4 and M, respectively.

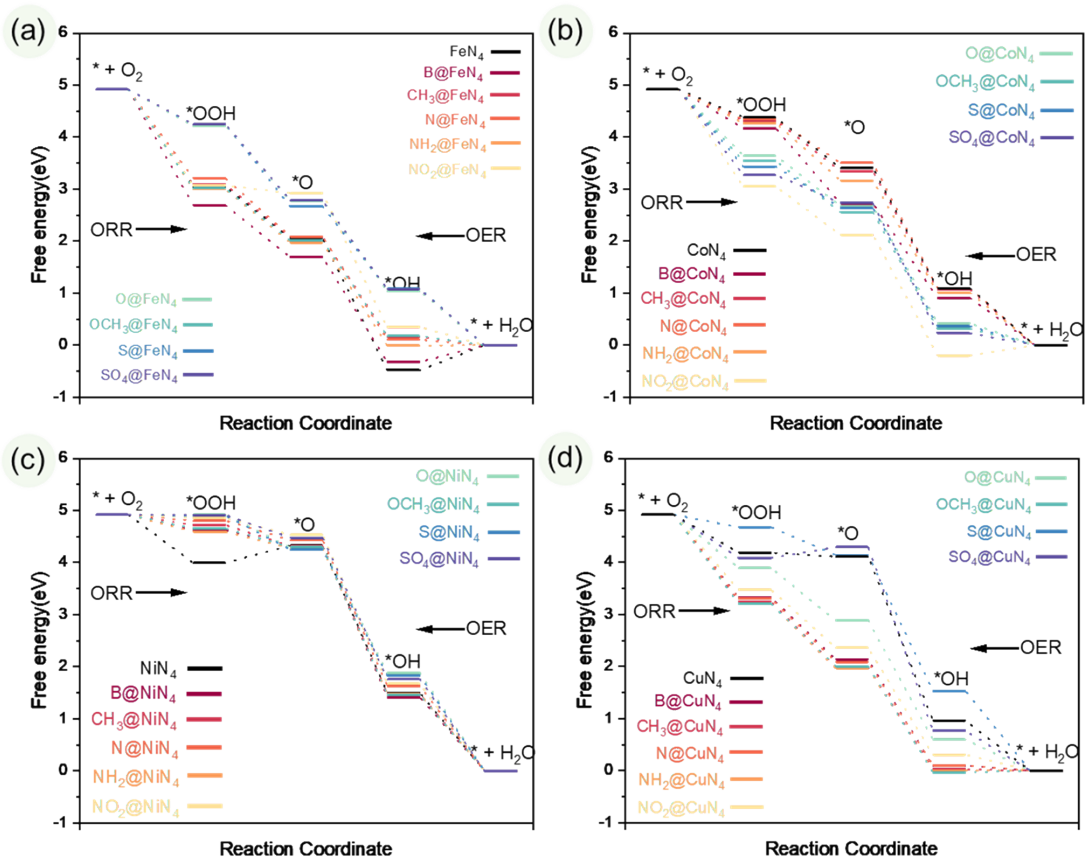

Figure S7. Free energy diagrams for ORR/OER on (a) Sub@FeN_4, (b) Sub@CoN_4, (c) SubNiN_4, and (d) Sub@CuN_4 catalysts

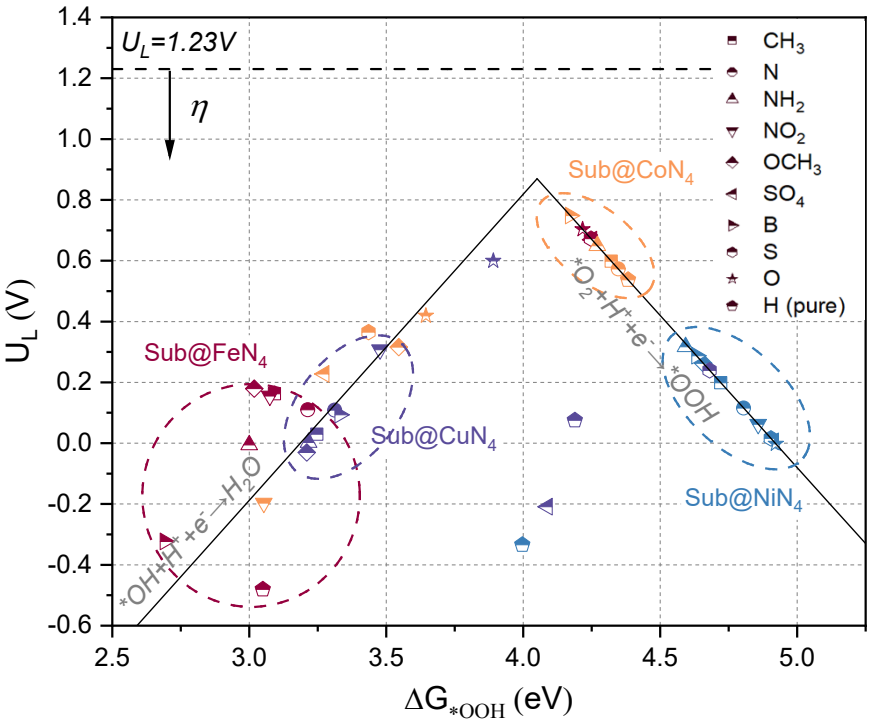

Figure S8. Volcano plots for ORR on Sub@FeN_4, Sub@CoN_4, SubNiN_4, and Sub@CuN_4.

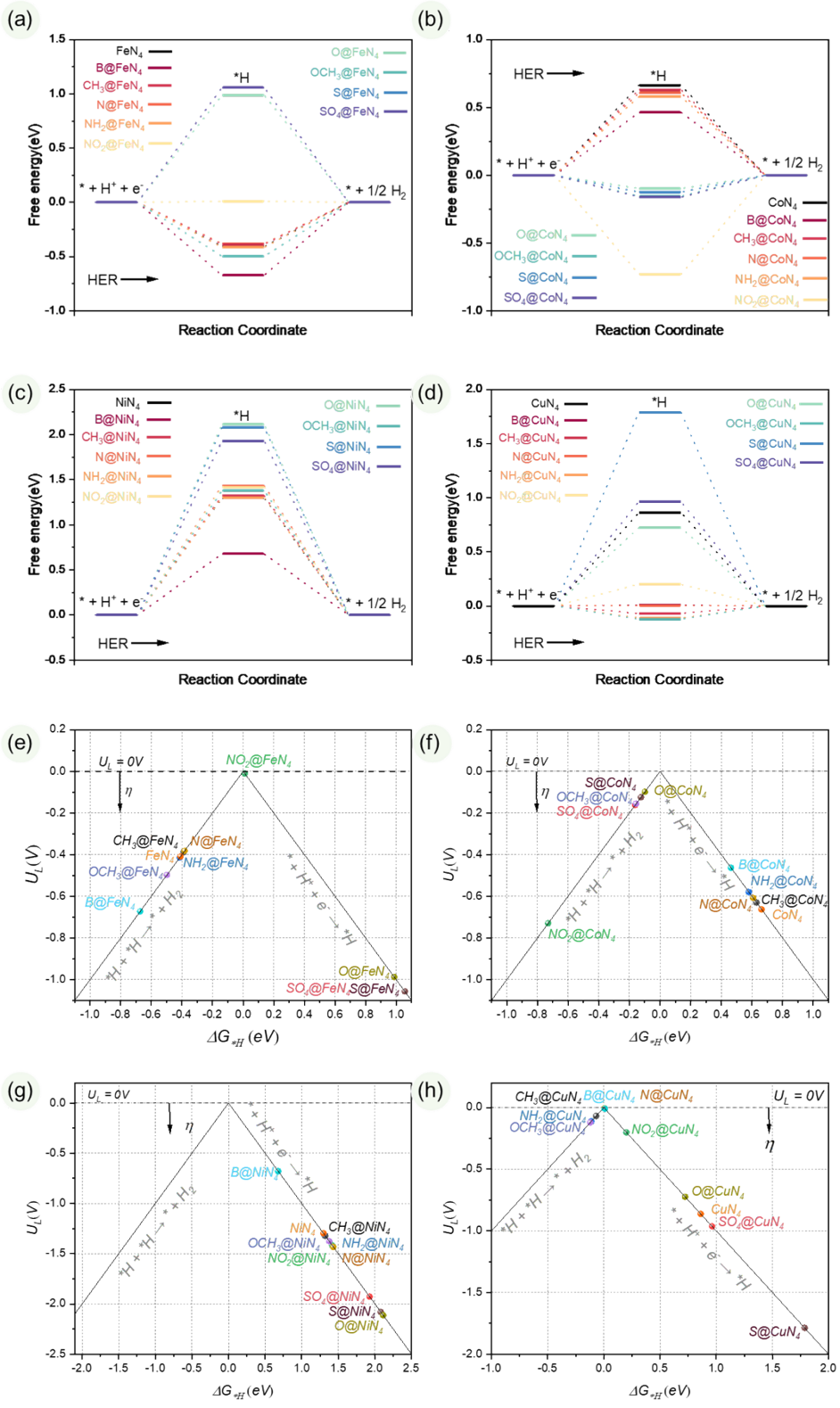

Figure S9. Free energy diagrams for HER on (a) Sub@FeN_4, (b) Sub@CoN_4, (c) SubNiN_4, and (d) Sub@CuN_4 catalysts; Volcano plots for HER on (e) Sub@FeN_4, (f) Sub@CoN_4, (g) SubNiN_4, and (h) Sub@CuN_4 catalysts.

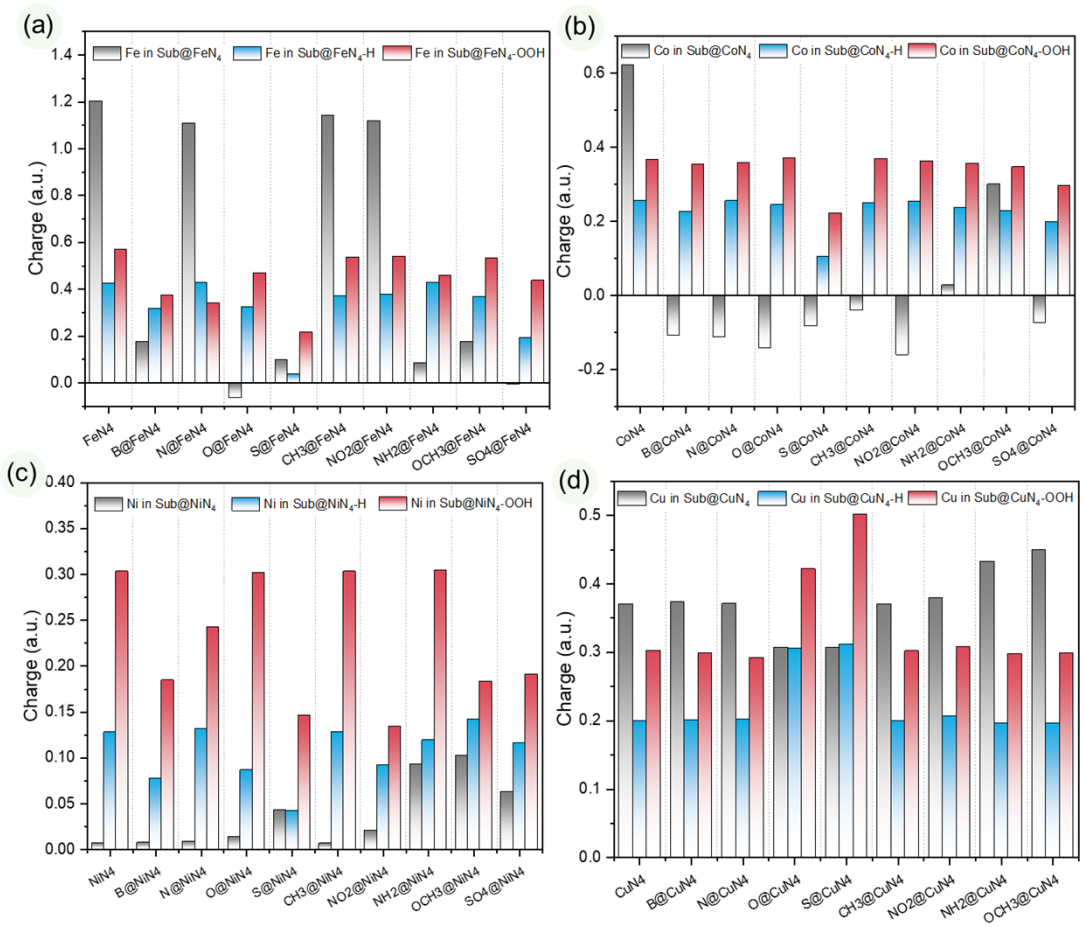

Figure S10. Variation of metal center charge in (a) Sub@FeN_4, (b) Sub@CoN_4, (c) Sub@NiN_4, and (d) Sub@CuN_4 catalysts with different edge-doping groups.

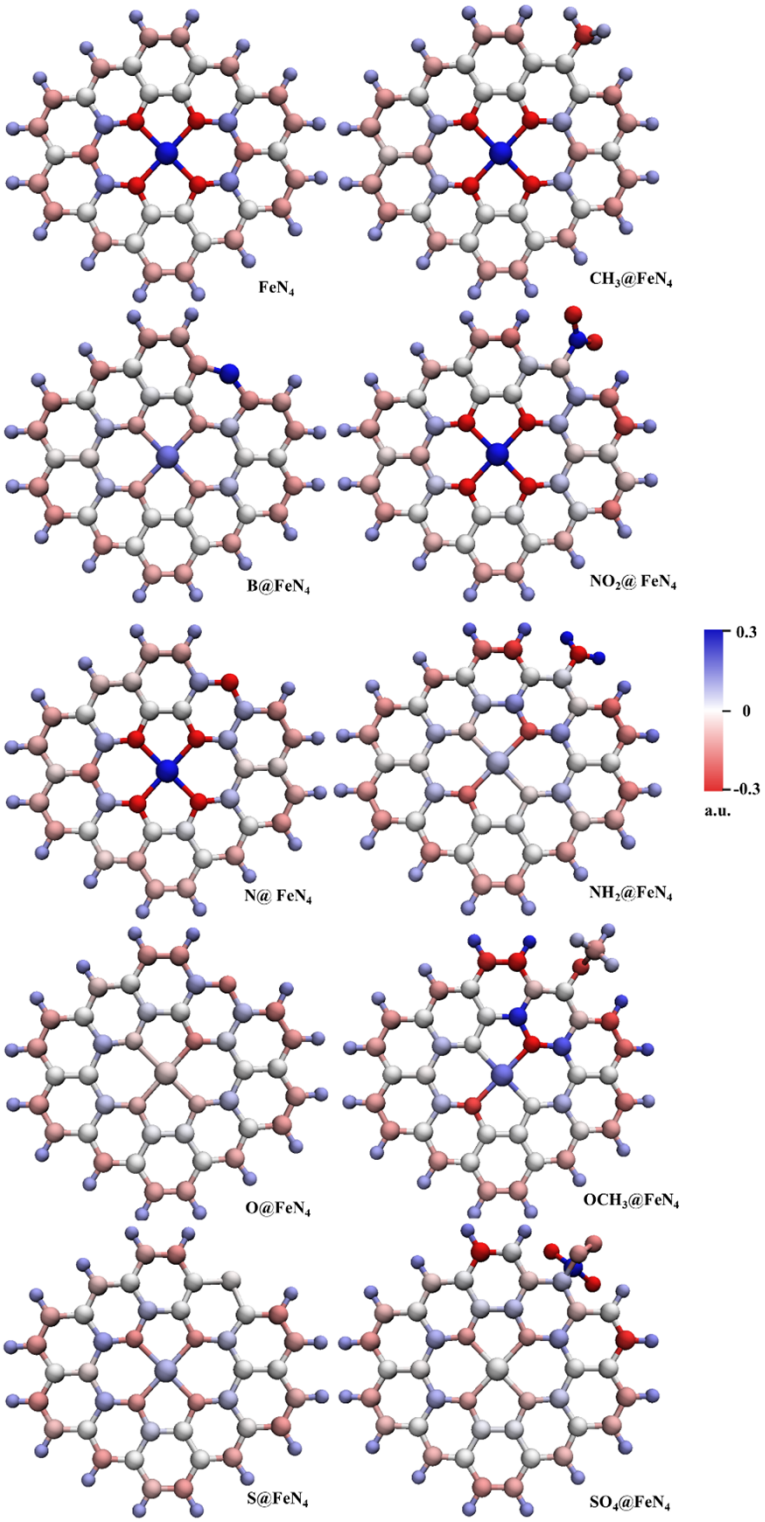

Figure S11. Charge distribution map of Sub@FeN_4 catalyst.

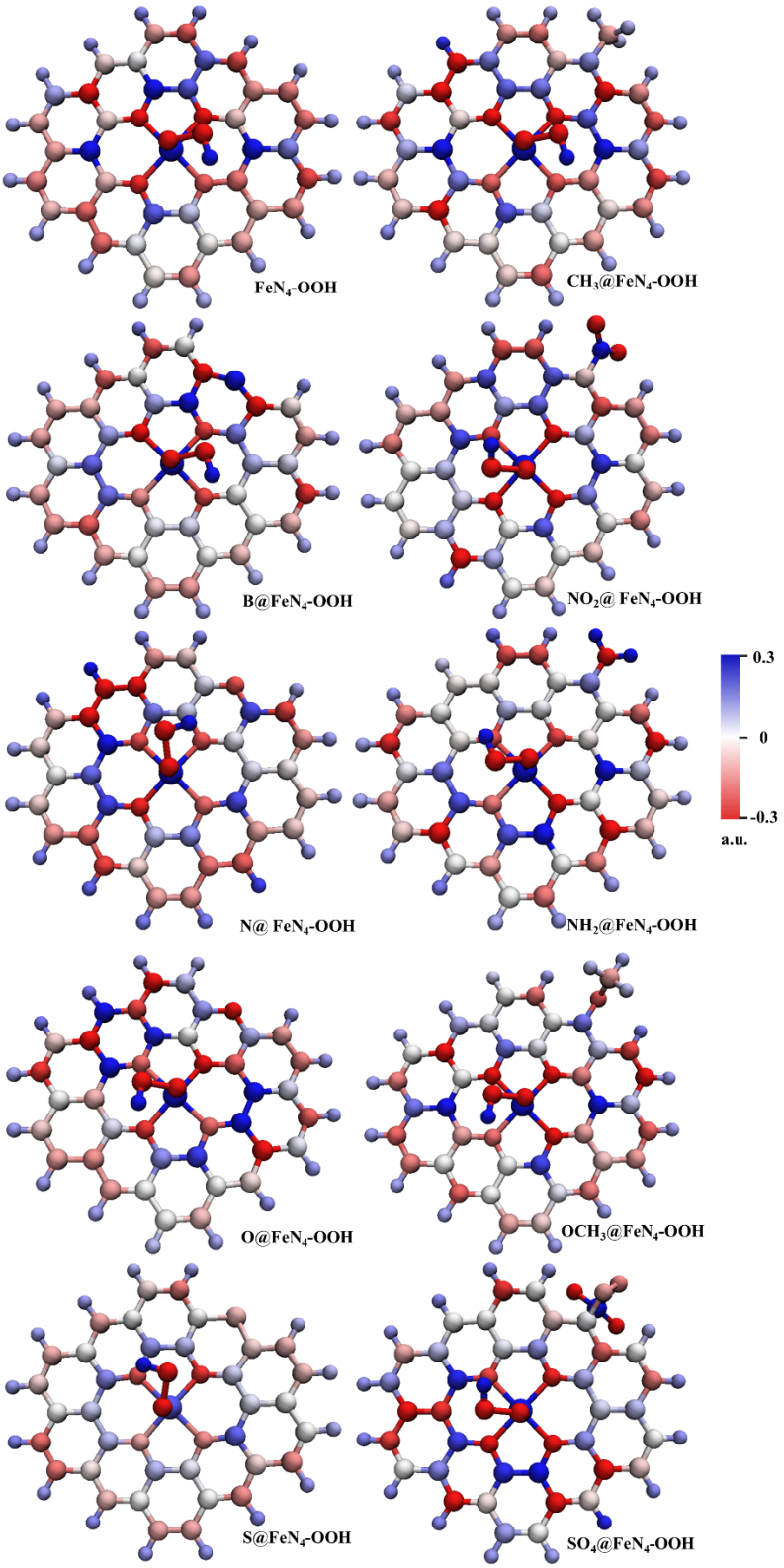

Figure S12. Charge distribution map of Sub@FeN_4 catalyst after *OOH adsorption.

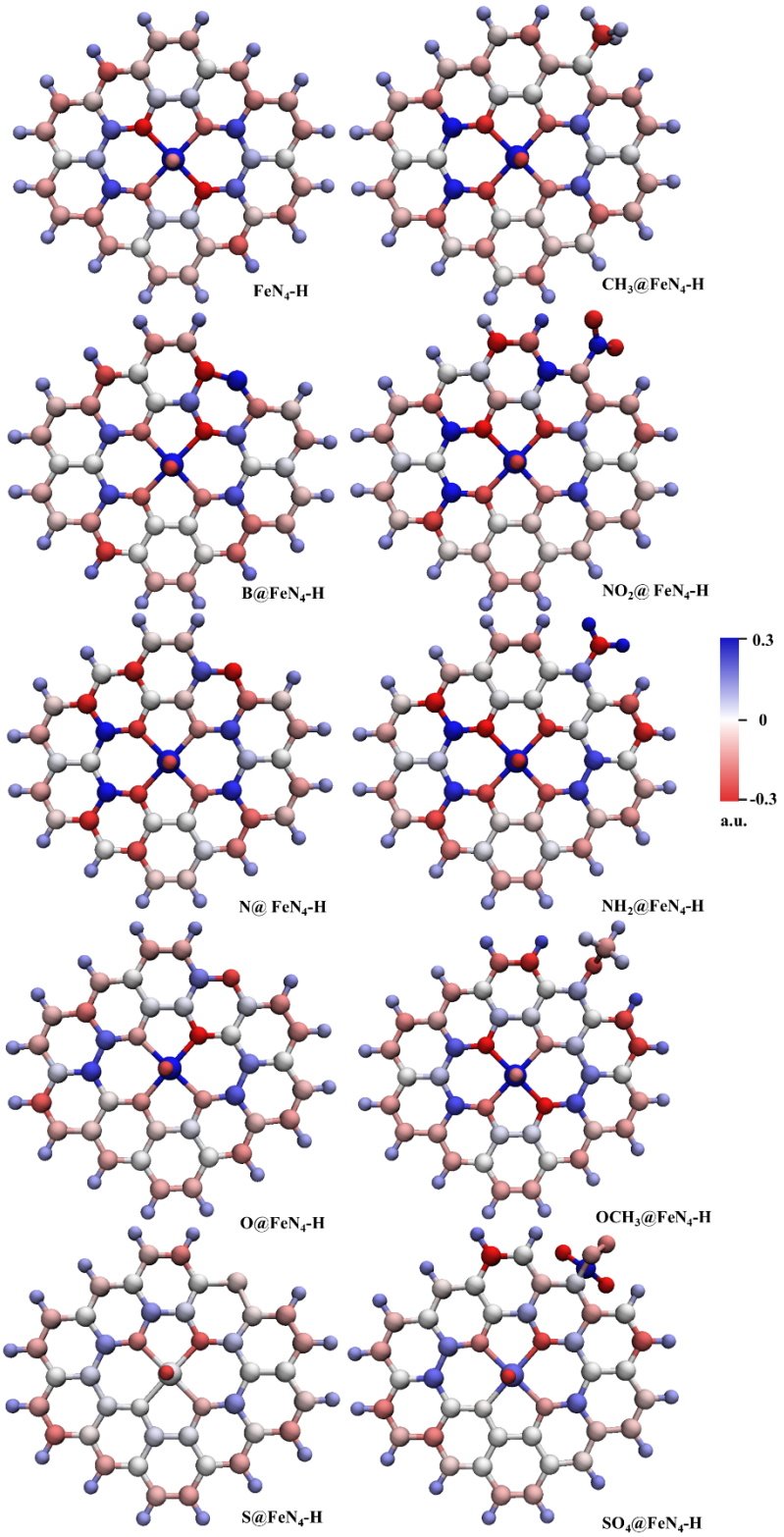

Figure S13. Charge distribution map of Sub@FeN_4 catalyst after *H adsorption.

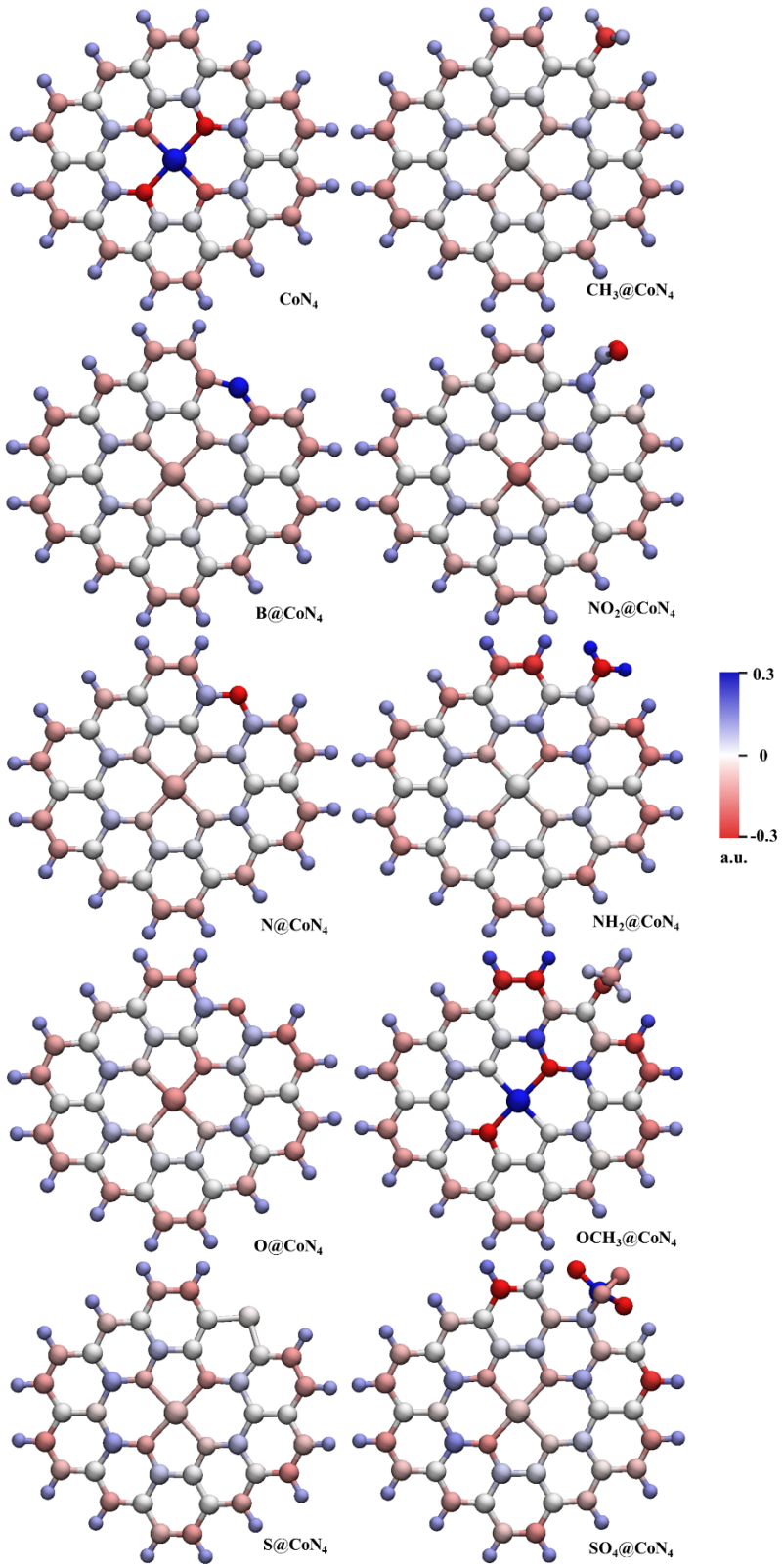

Figure S14. Charge distribution map of Sub@CoN_4 catalyst.

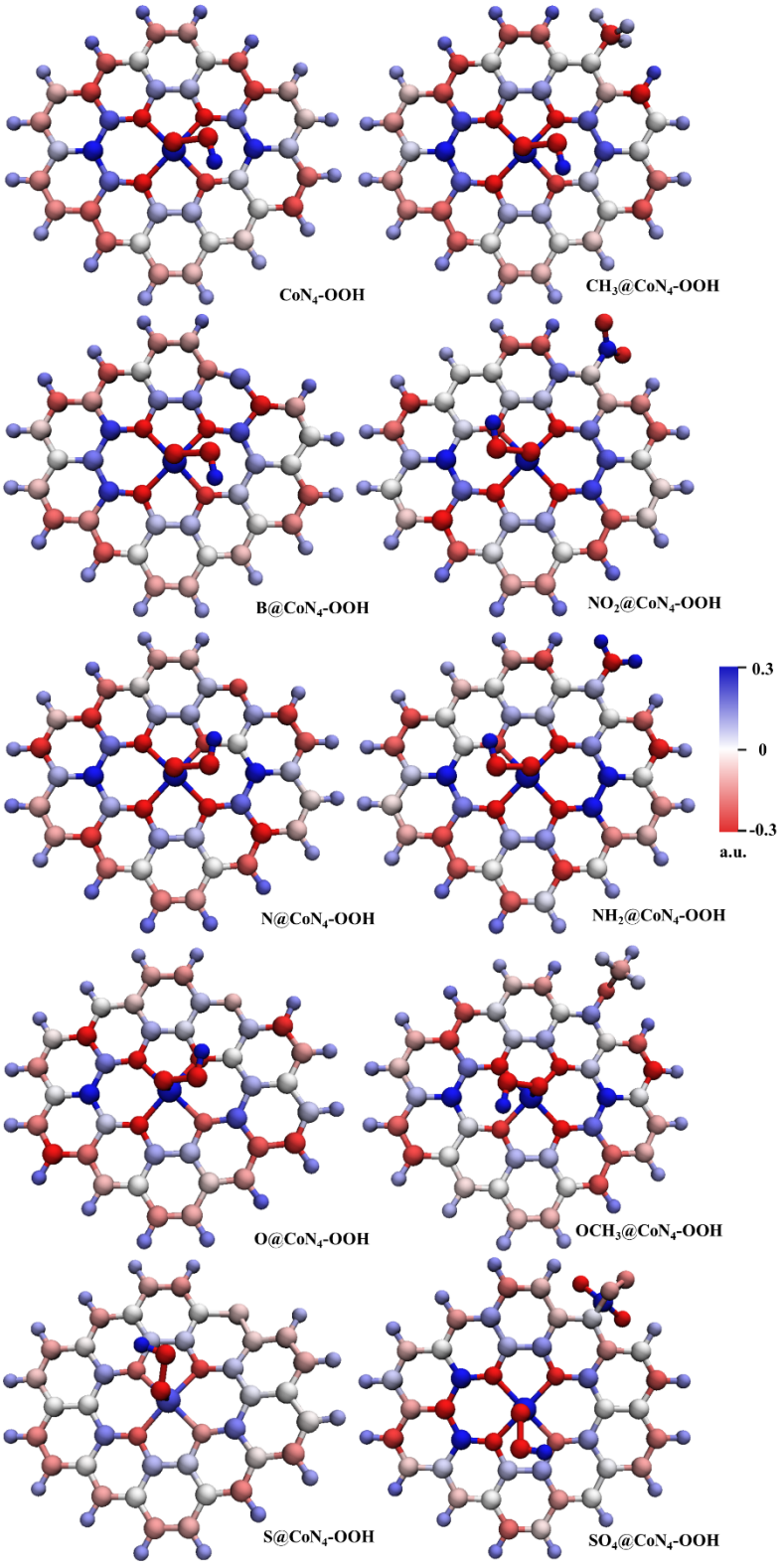

Figure S15. Charge distribution map of Sub@CoN_4 catalyst after *OOH adsorption.

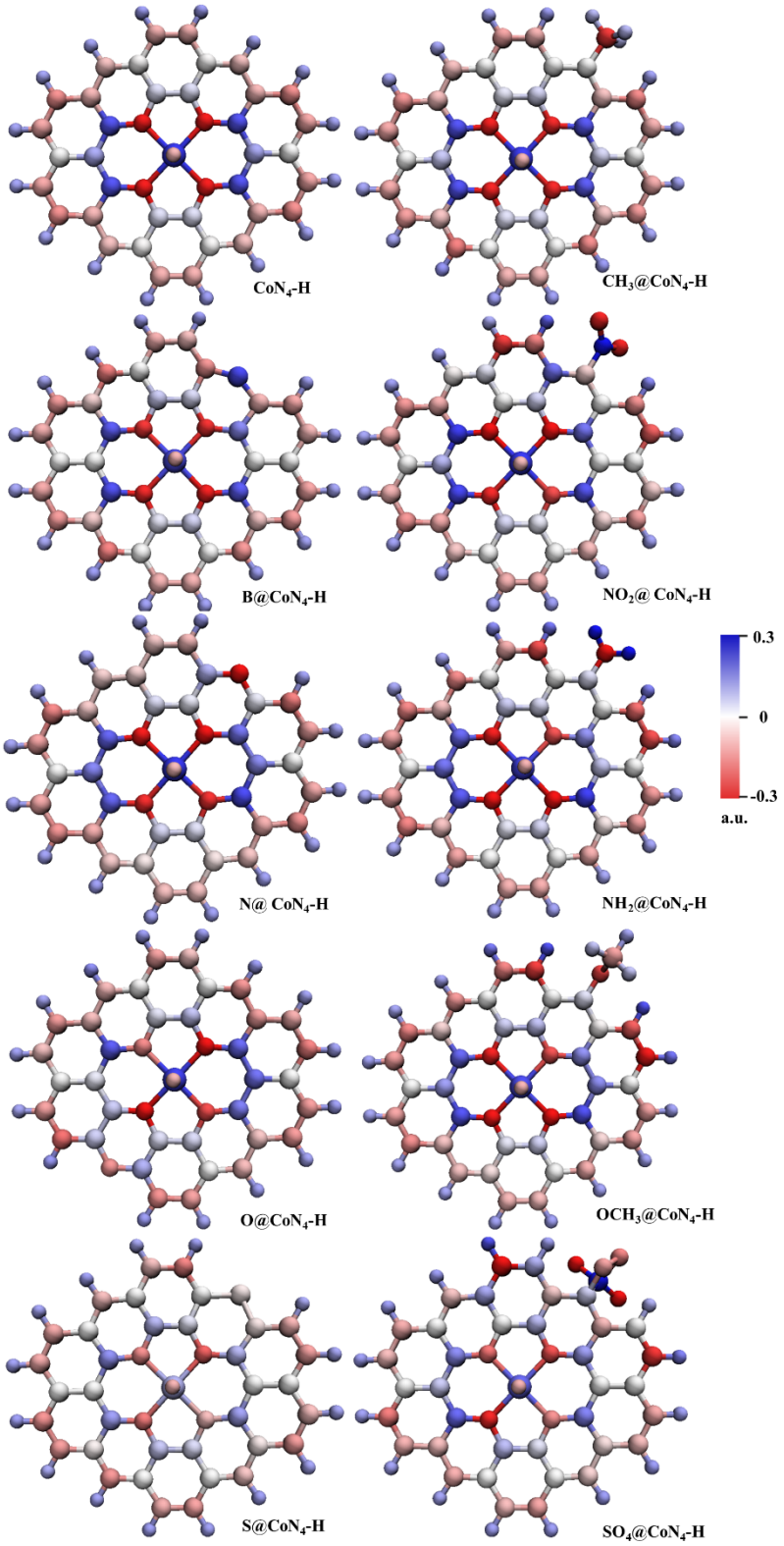

Figure S16. Charge distribution map of Sub@CoN_4 catalyst after *H adsorption.

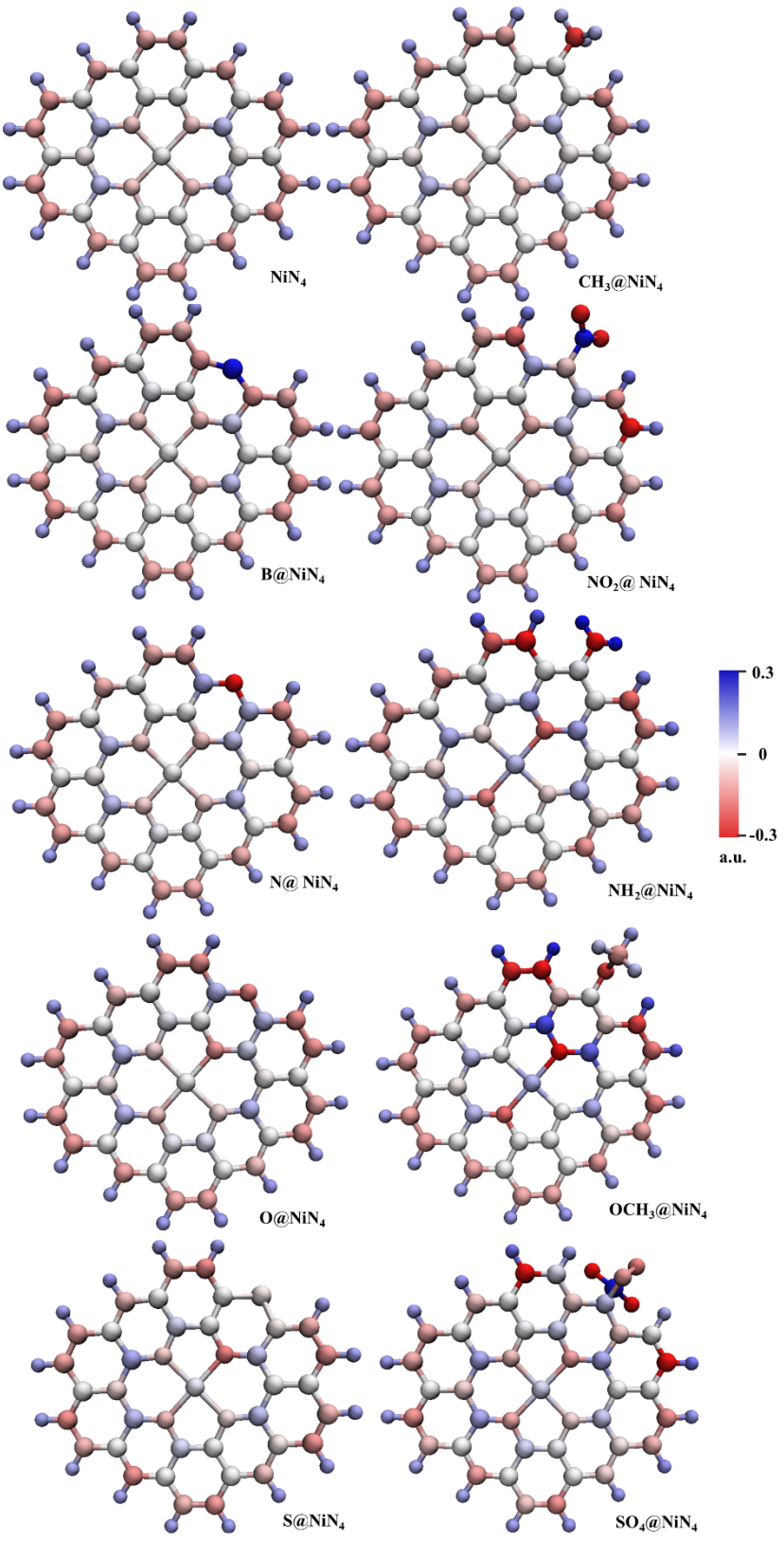

Figure S17. Charge distribution map of Sub@NiN_4 catalyst.

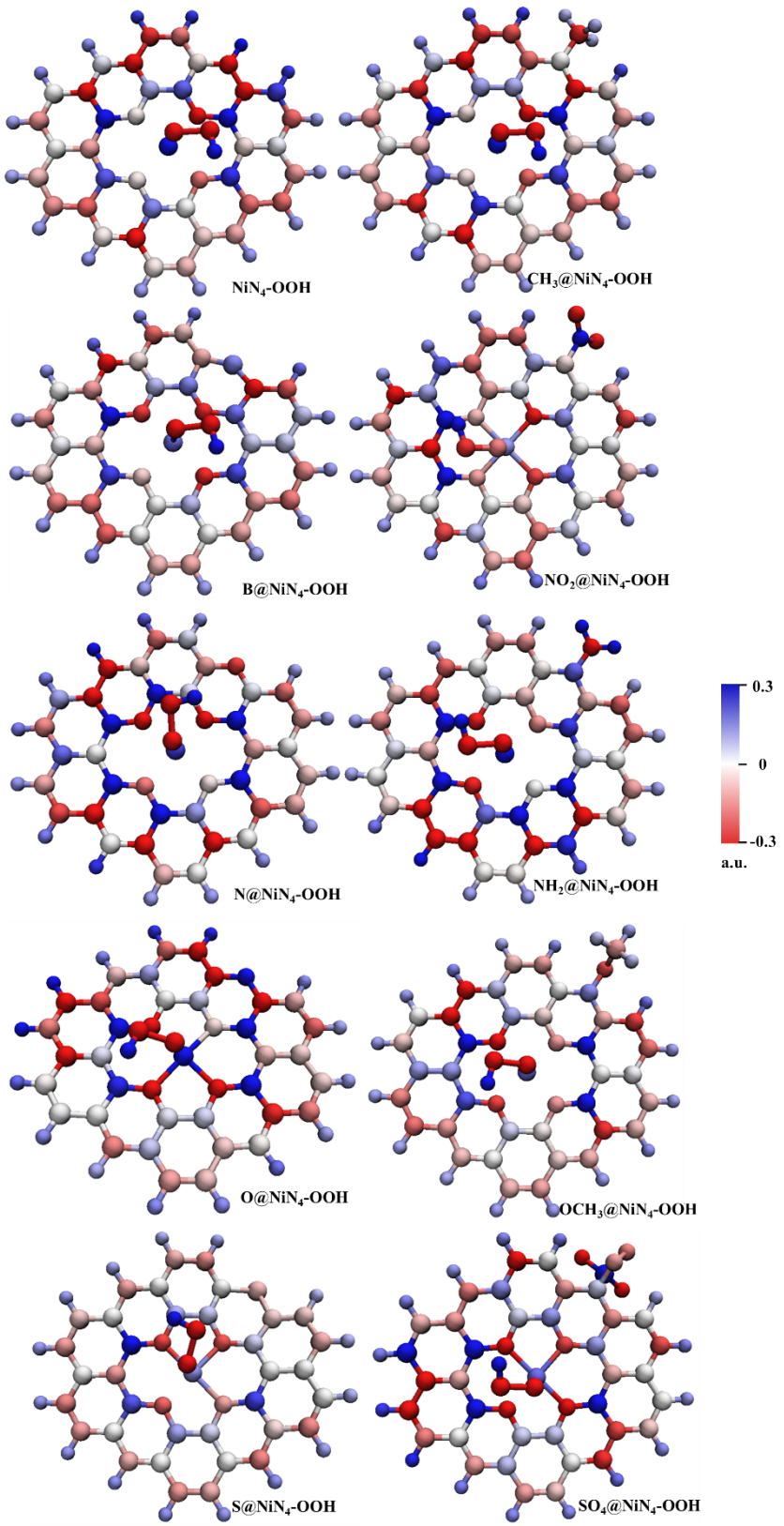

Figure S18. Charge distribution map of Sub@NiN_4 catalyst with *OOH adsorption.

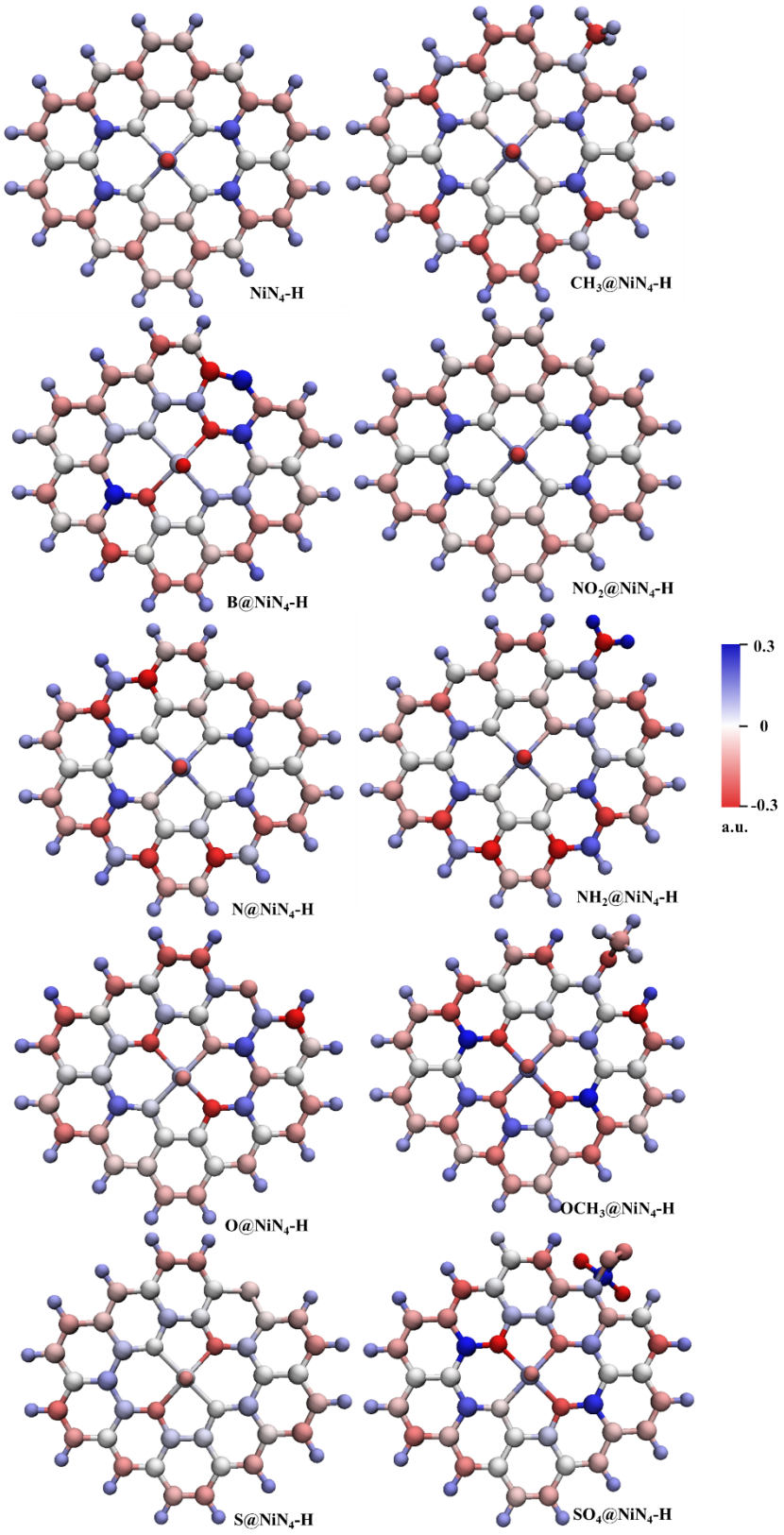

Figure S19. Charge distribution map of Sub@NiN_4 catalyst with *H adsorption.

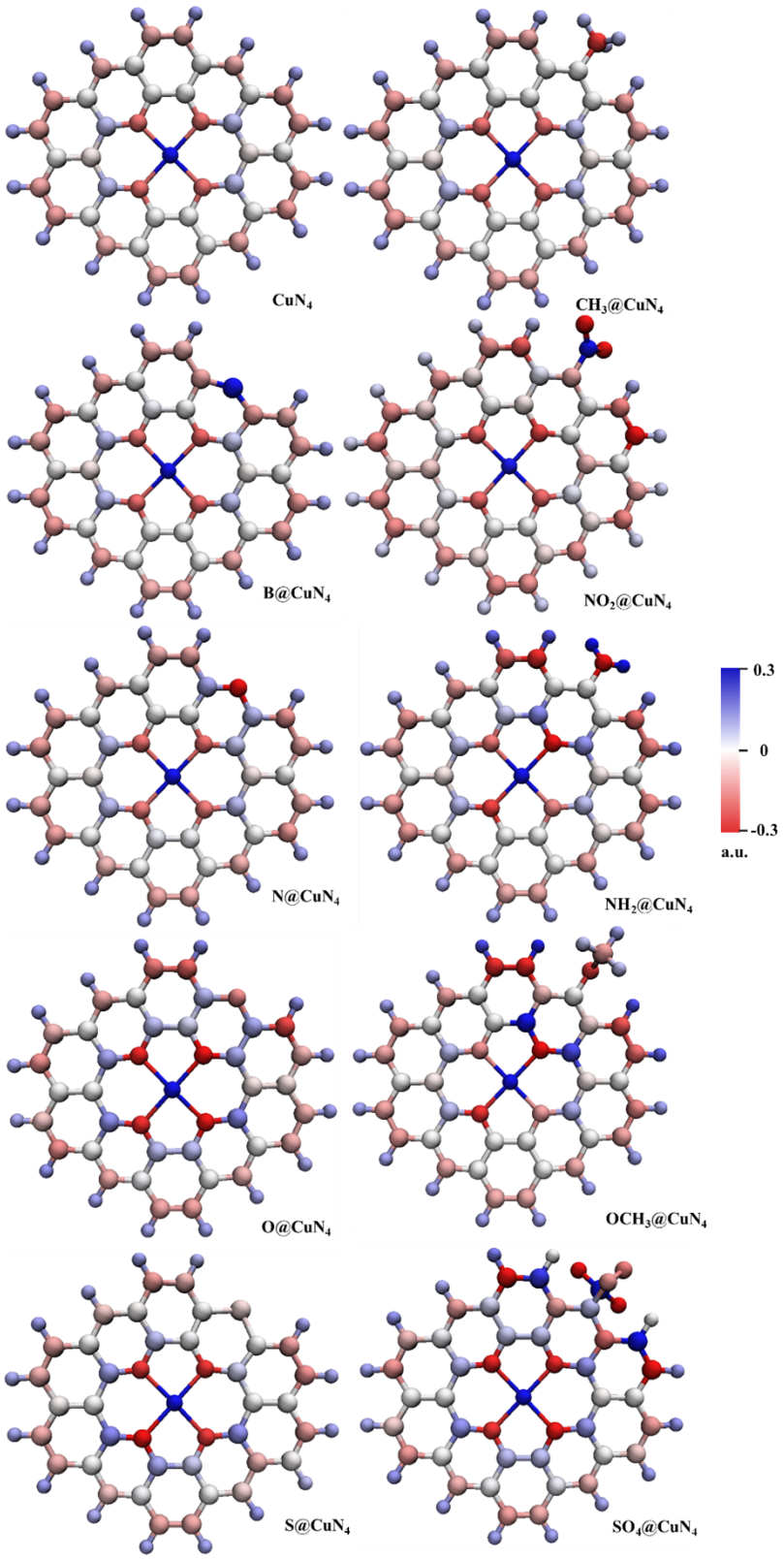

Figure S20. Charge distribution map of Sub@CuN_4 catalyst.

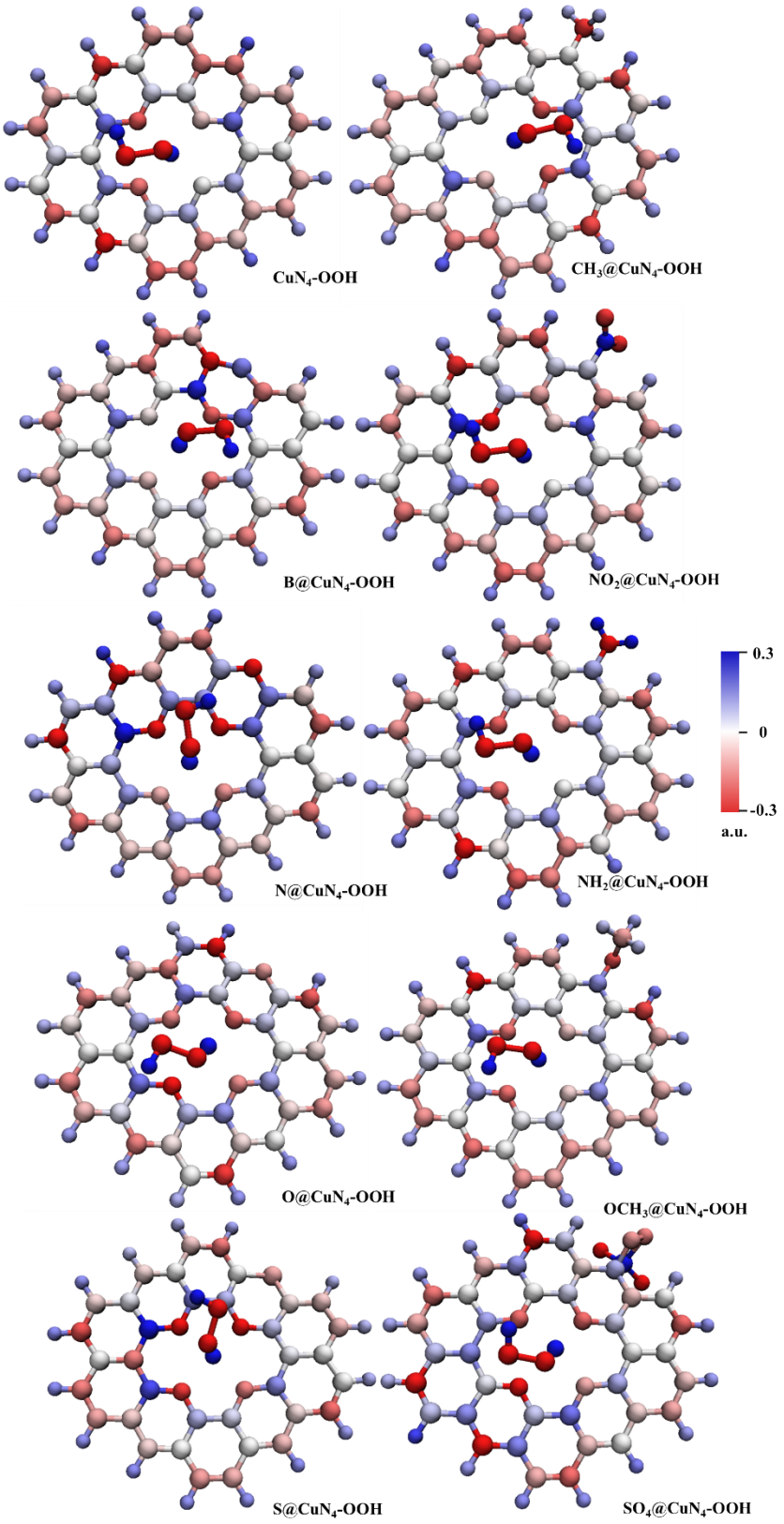

Figure S21. Charge distribution map of Sub@CuN_4 catalyst with *OOH adsorption.

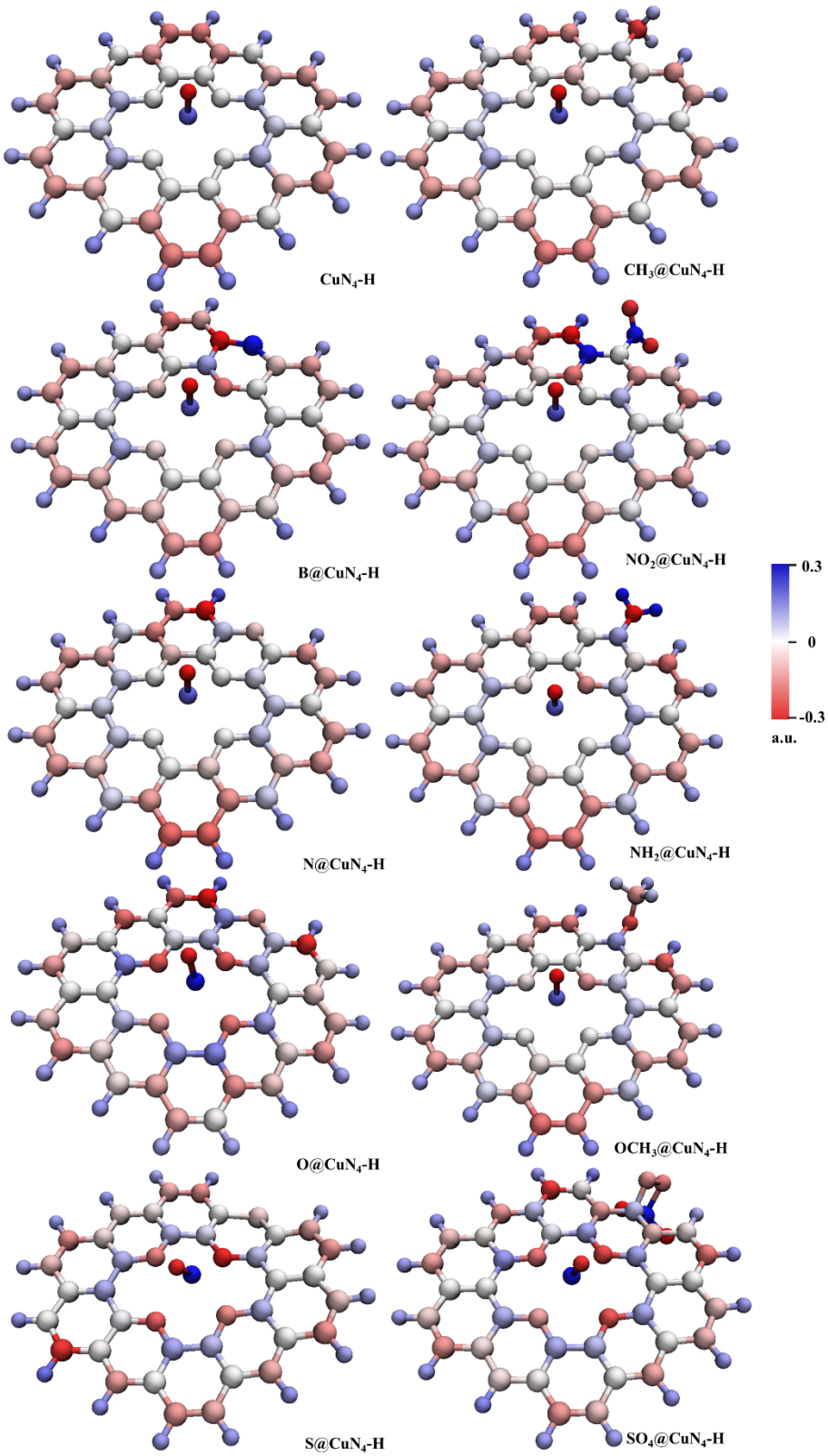

Figure S22. Charge distribution map of Sub@CuN_4 catalyst with *H adsorption.

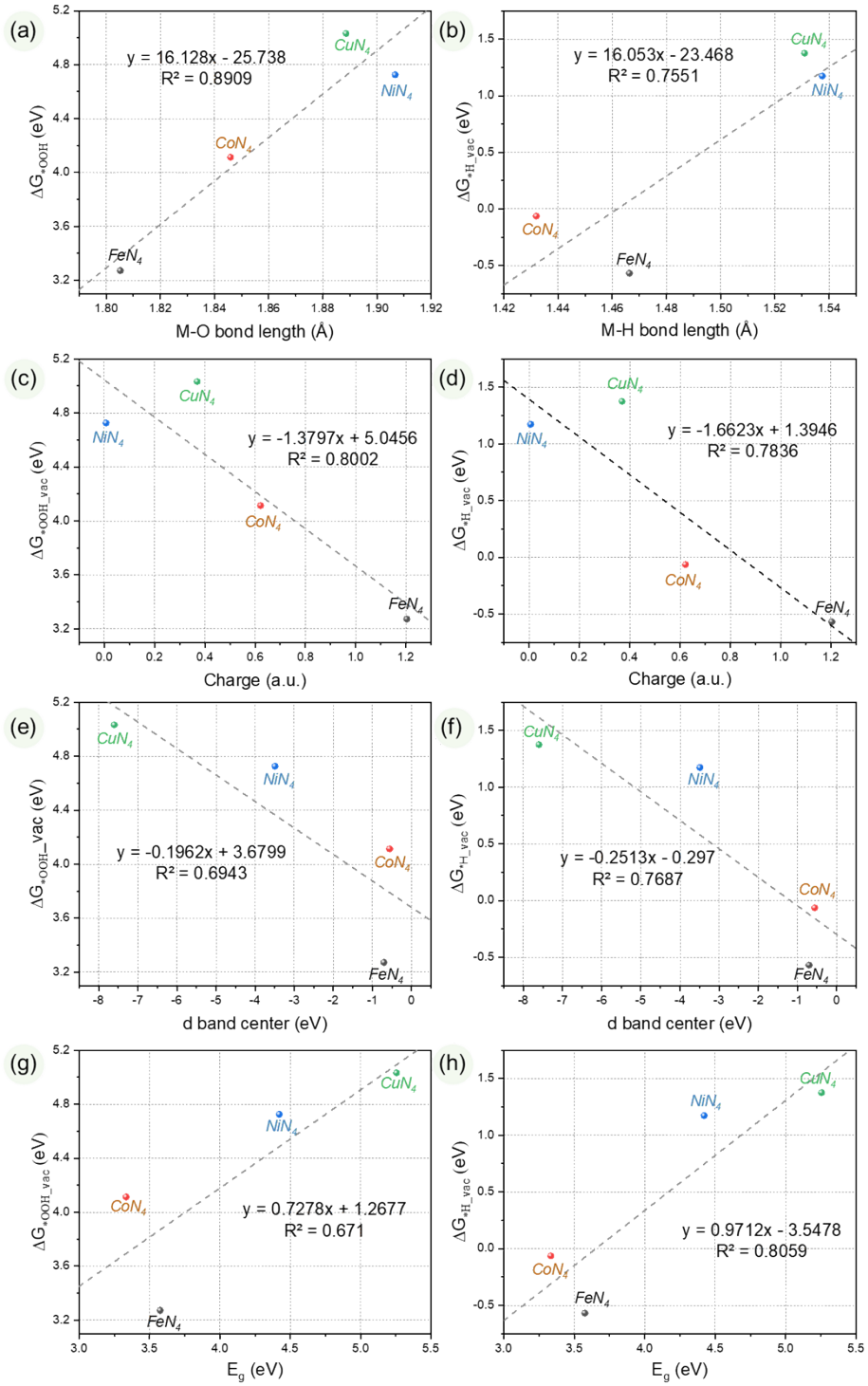

Figure S23. Structure-activity relationships in MN_4. Correlation of *OOH adsorption free energy with (a) M-O bond length, (b) metal center charge, (c) d-band center, and (d) fundamental gap; correlation of *H adsorption free energy with (e) M-H bond length, (f) metal center charge, (g) d-band center, and (h) fundamental gap.

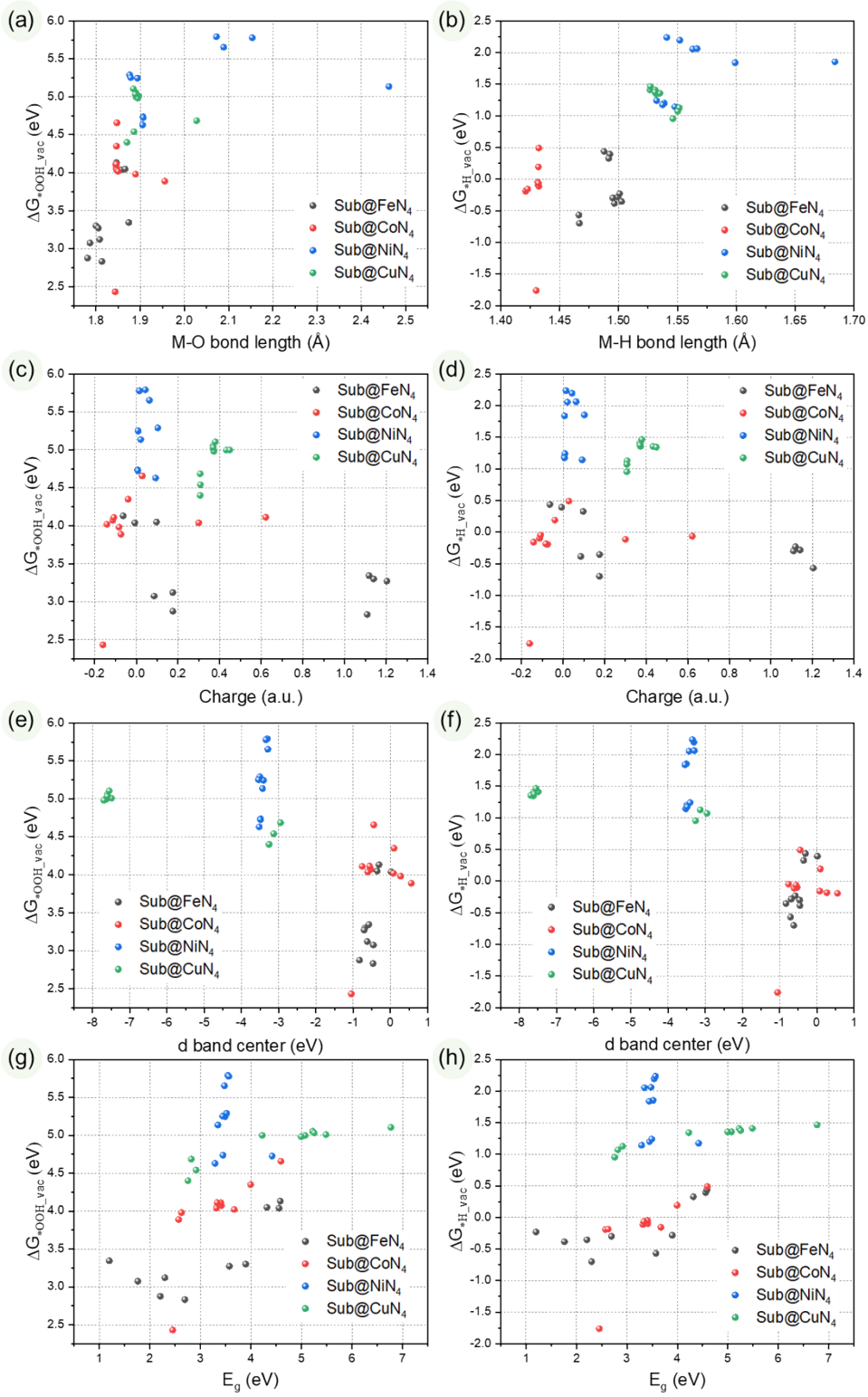

Figure S24. Structure-activity relationships in Sub@MN_4. Correlation of *OOH adsorption free energy with (a) M-O bond length, (b) metal center charge, (c) d-band center, and (d) fundamental gap; correlation of *H adsorption free energy with (e) M-H bond length, (f) metal center charge, (g) d-band center, and (h) fundamental gap.

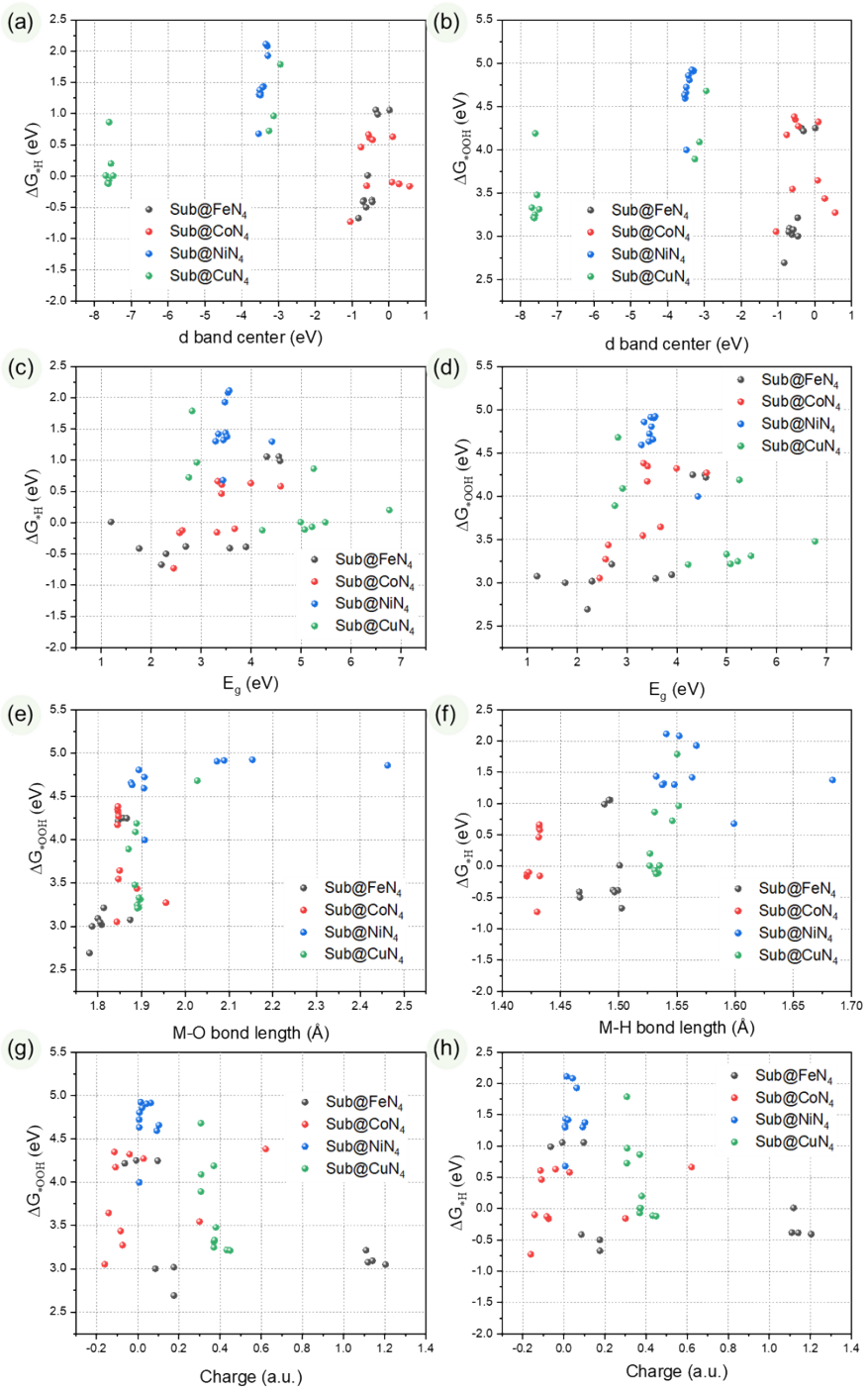

Figure S25. Structure-activity relationships in Sub@MN_4 considering the implicit solvent model. Correlation of *OOH adsorption free energy with (a) M-O bond length, (b) metal center charge, (c) d-band center, and (d) fundamental gap; correlation of *H adsorption free energy with (e) M-H bond length, (f) metal center charge, (g) d-band center, and (h) fundamental gap.

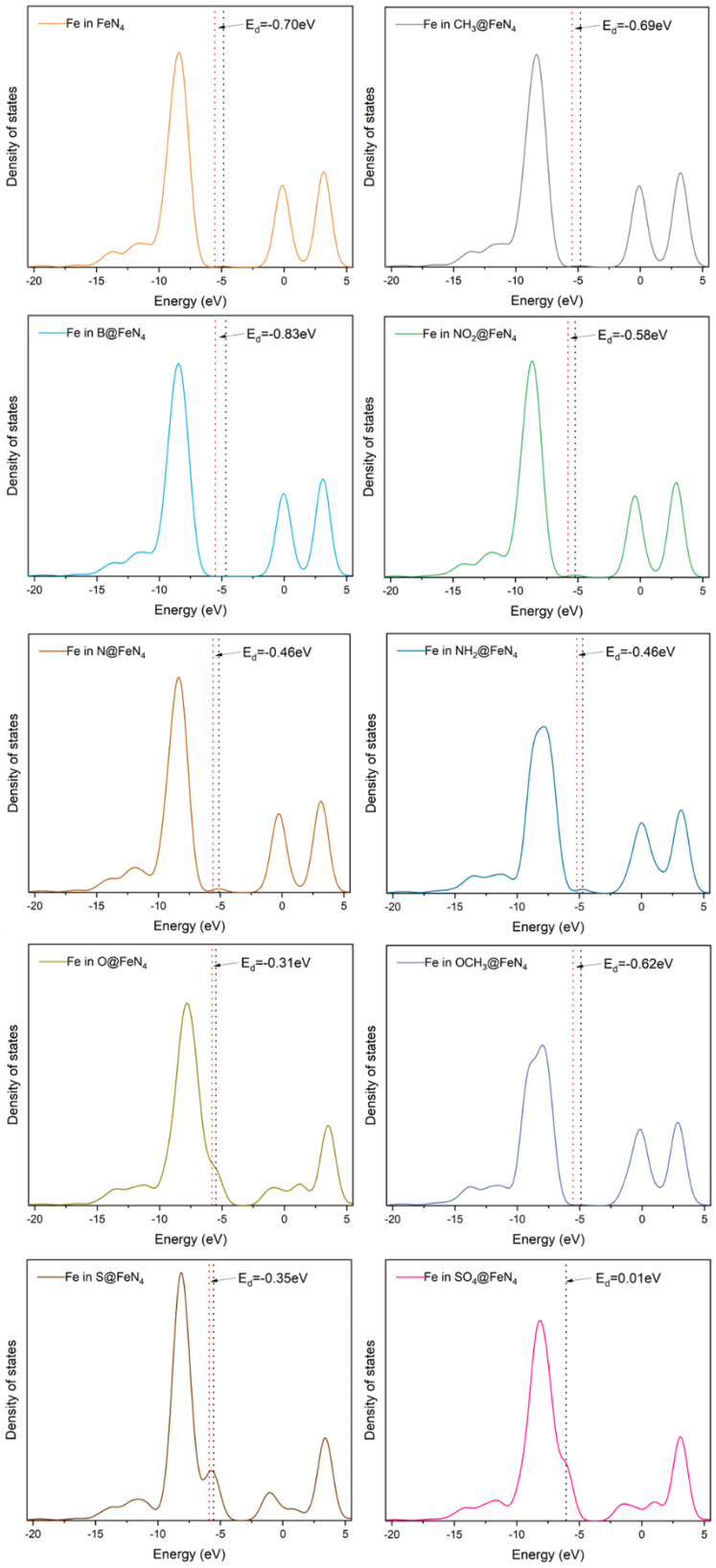

Figure S26. d-band center of Fe in Sub@FeN_4 catalyst.

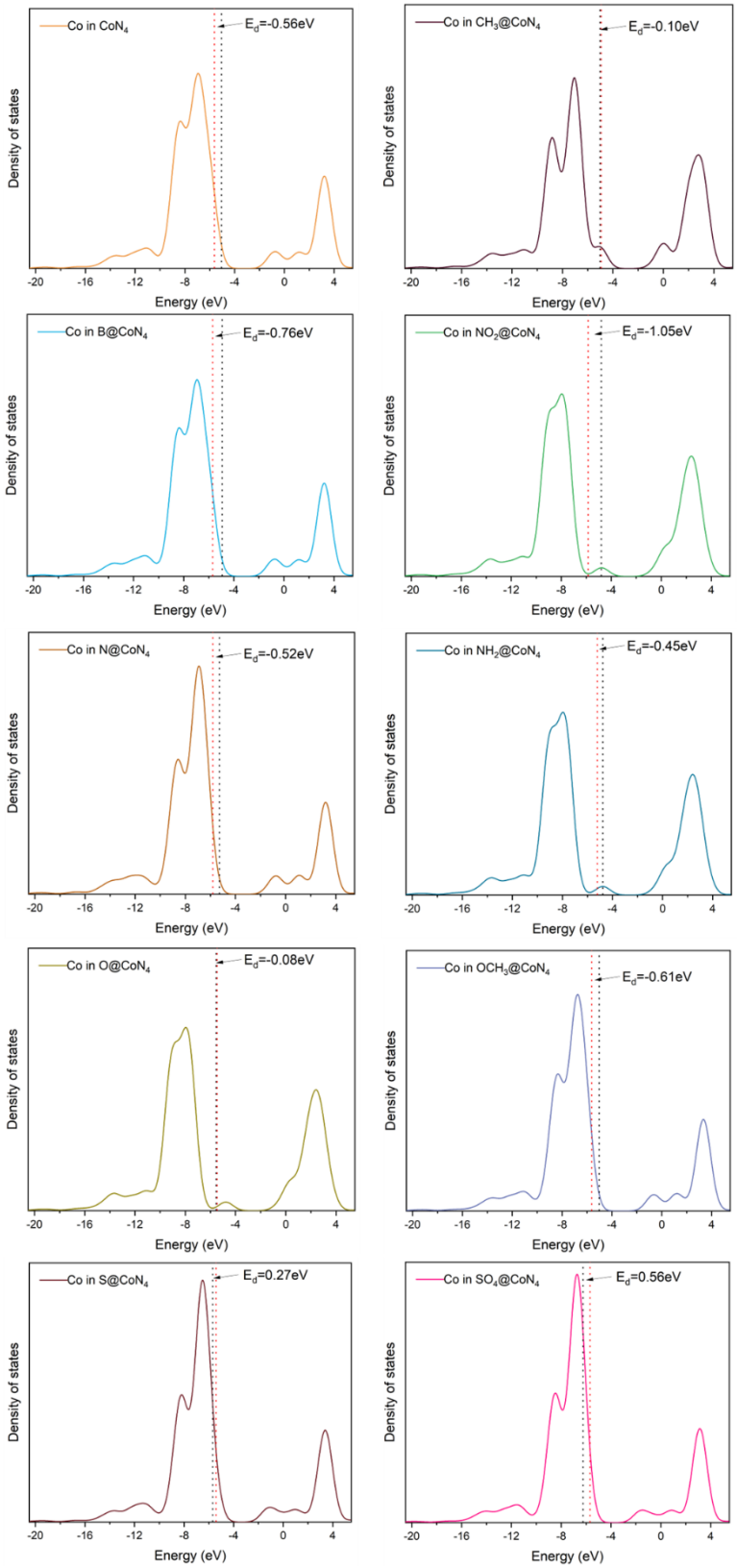

Figure S27. d-band center of Co in Sub@CoN_4 catalyst.

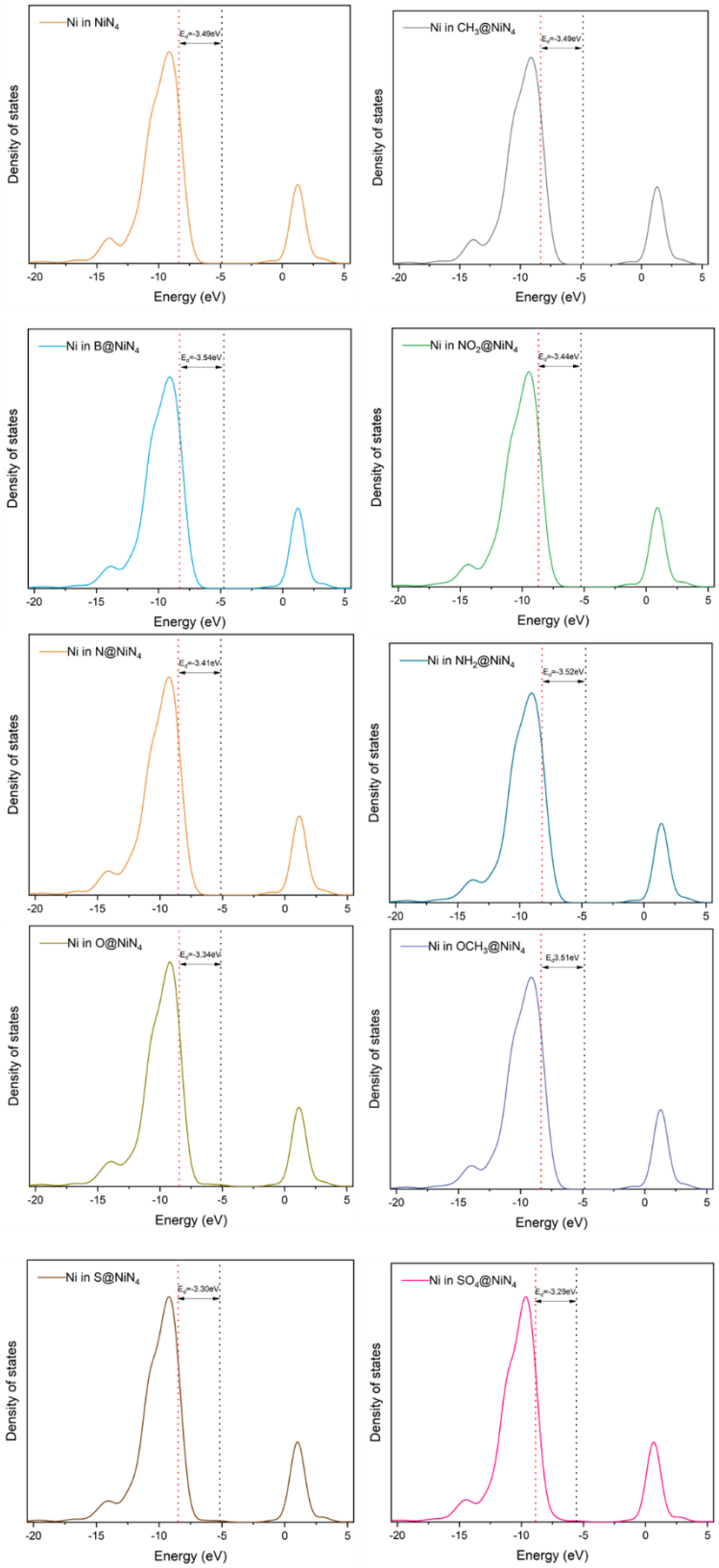

Figure S28. d-band center of Ni in Sub@NiN_4 catalyst.

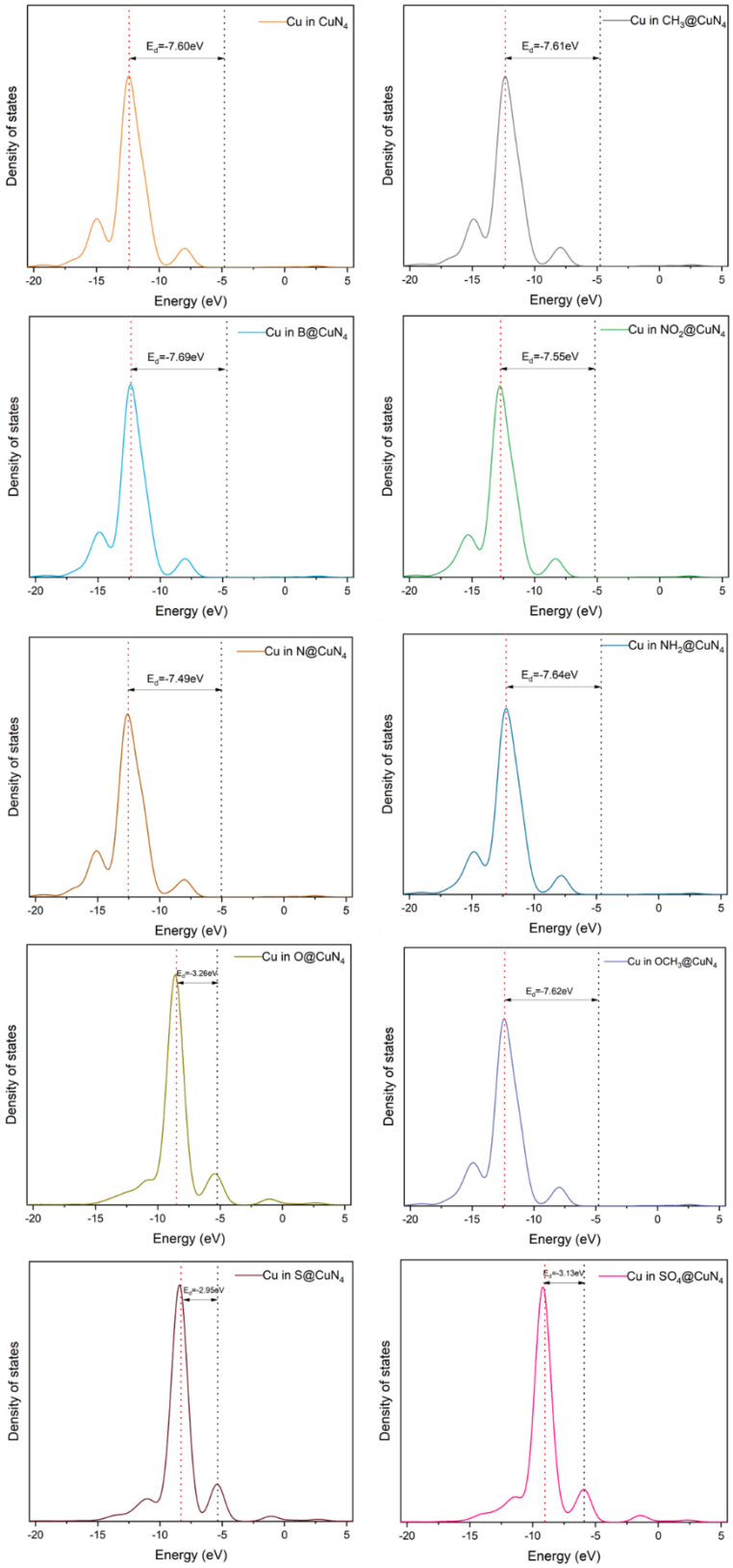

Figure S29. d-band center of Cu in Sub@CuN_4 catalyst.

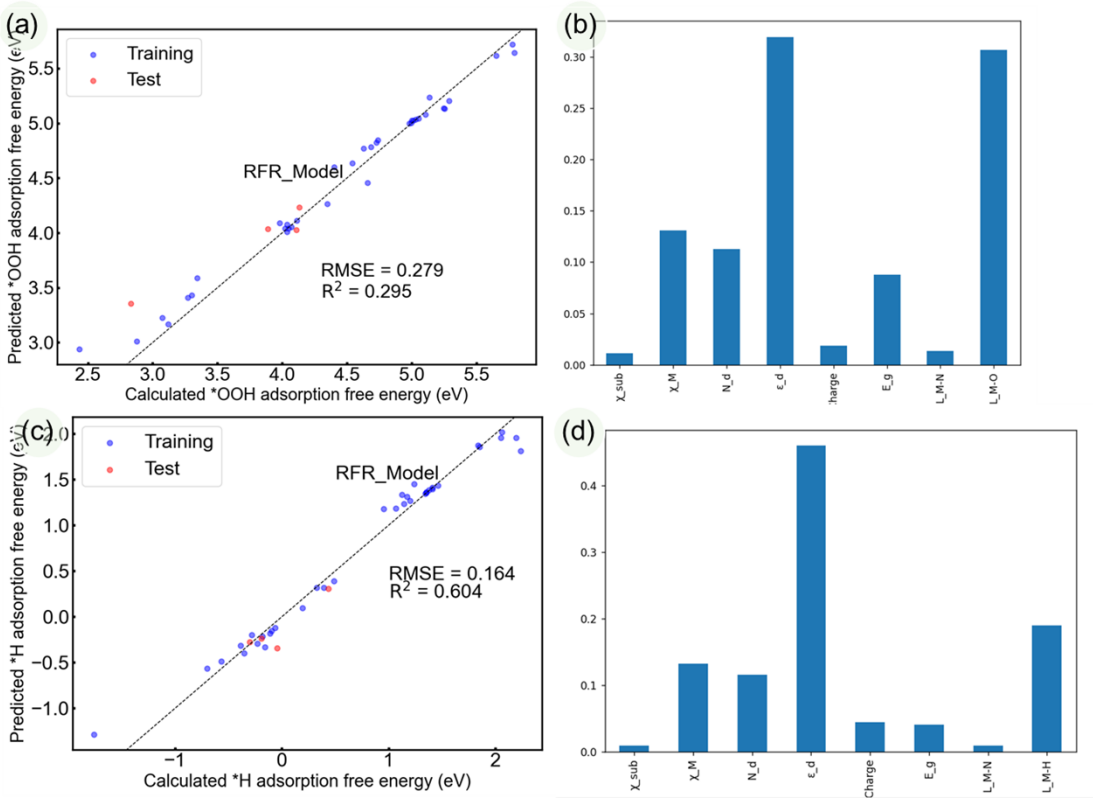

Figure S30. Comparison of (a) *OOH adsorption free energy and (c) *H adsorption free energy calculated from the Random Forest Regression (RFR) model with DFT (Density Functional Theory) computed values. Importance analysis of each feature for (b) *OOH adsorption free energy and (d) *H adsorption free energy.

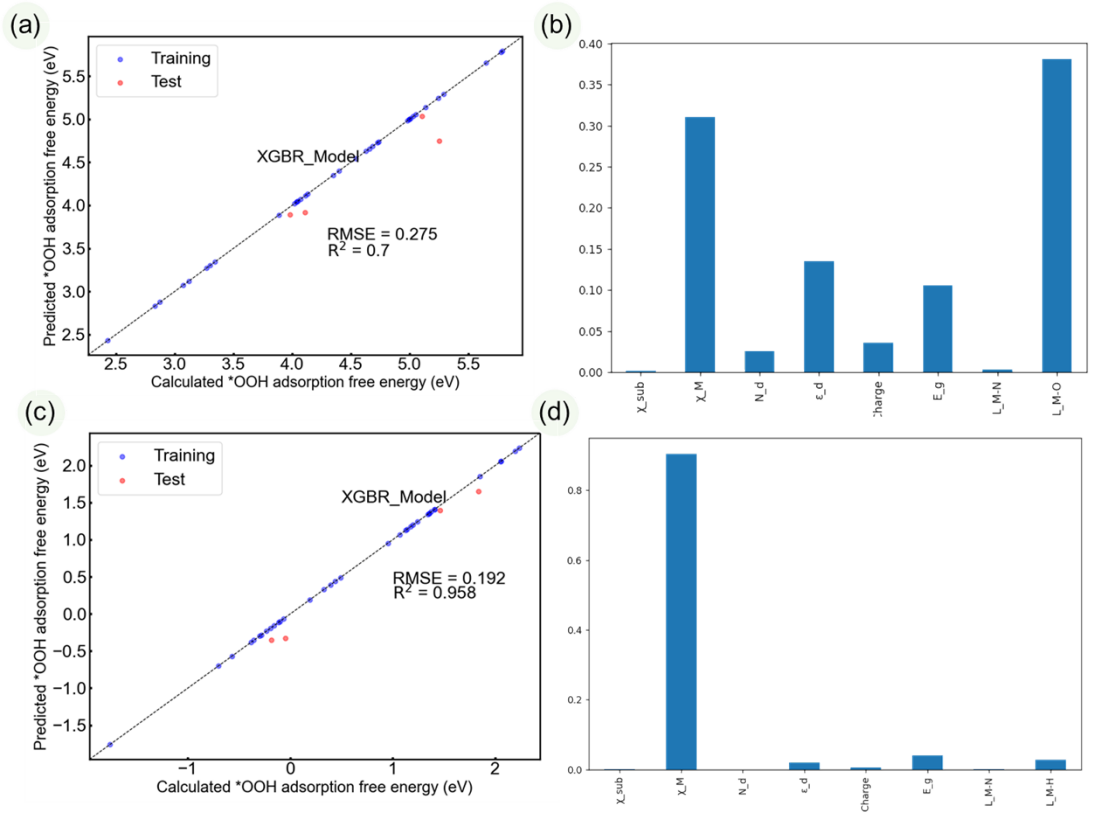

Figure S31. Comparison of (a) *OOH adsorption free energy and (c) *H adsorption free energy calculated from the XGBoost Regression (XGBR) model with DFT (Density Functional Theory) computed values. Importance analysis of each feature for (b) *OOH adsorption free energy and (d) *H adsorption free energy.

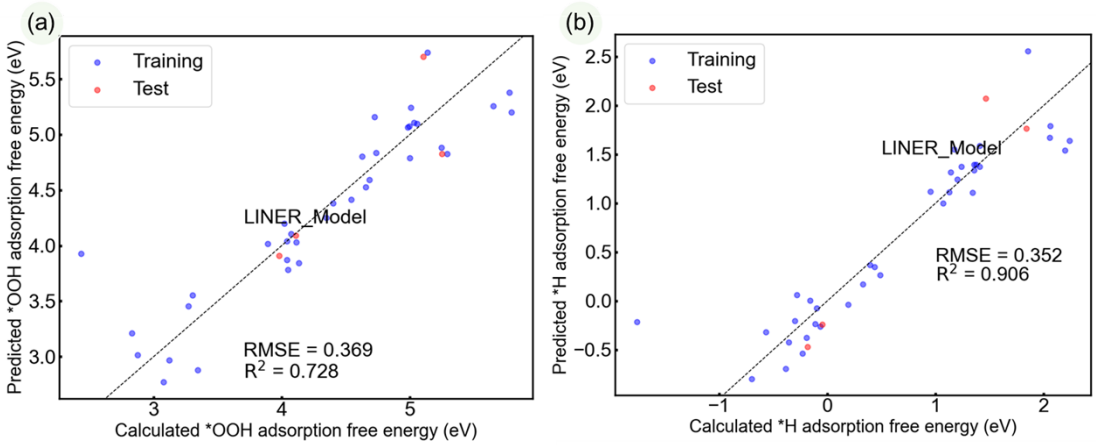

Figure S32. Comparison of (a) *OOH adsorption free energy and (b) *H adsorption free energy calculated from the LINER model with DFT (Density Functional Theory) computed values.

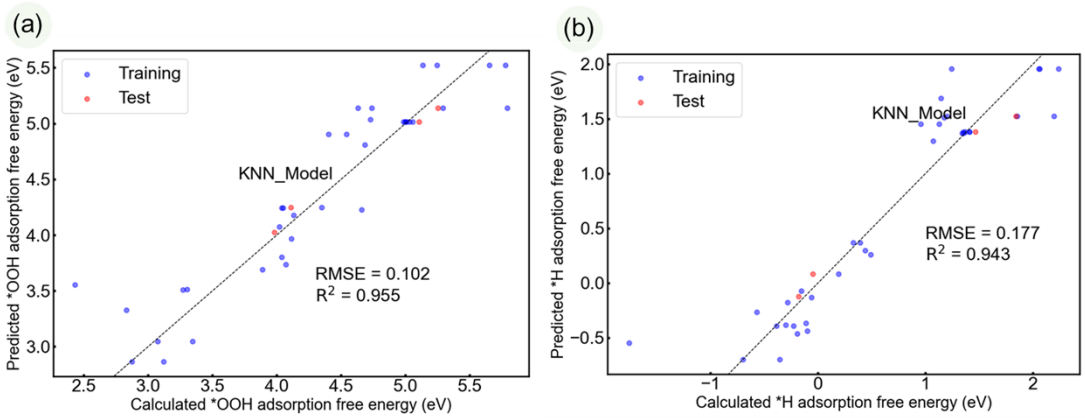

Figure S33. Comparison of (a) *OOH adsorption free energy and (b) *H adsorption free energy calculated from the KNN (K-Nearest Neighbors) model with DFT (Density Functional Theory) computed values.

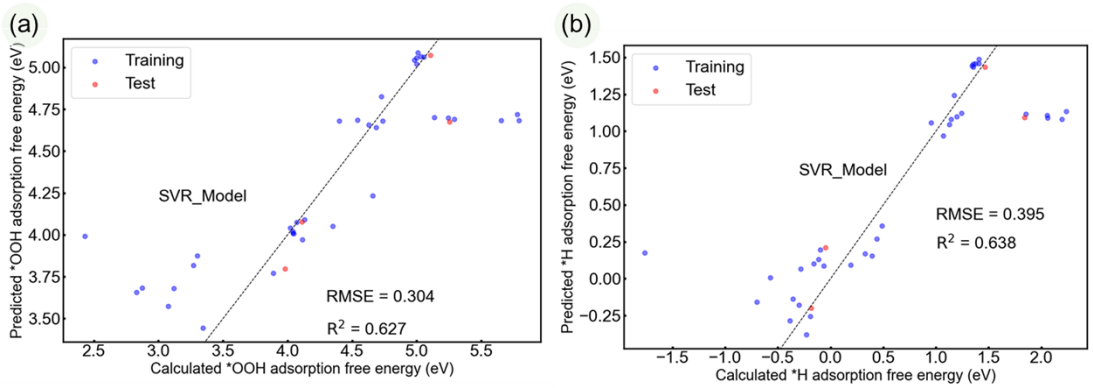

Figure S34. Comparison of (a) *OOH adsorption free energy and (b) *H adsorption free energy calculated from the SVR (Support Vector Regression) model with DFT (Density Functional Theory) computed values.

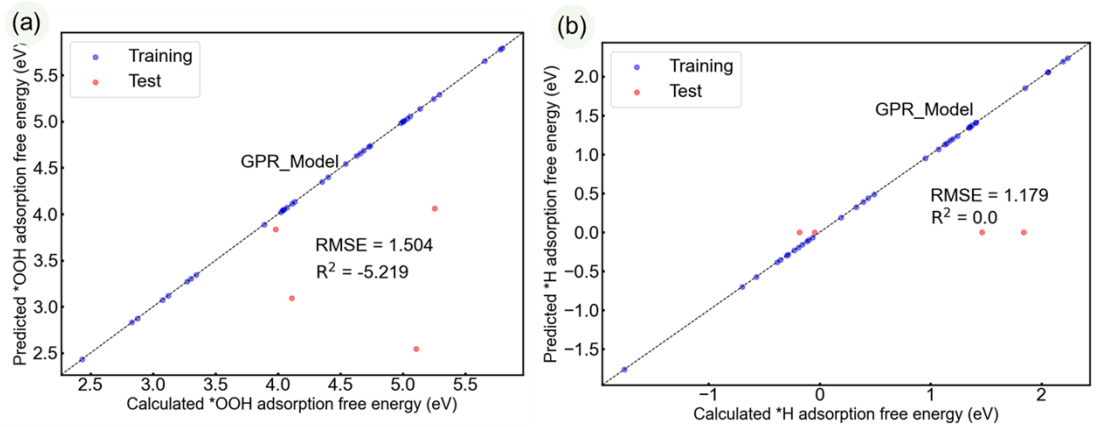

Figure S35. Comparison of (a) *H adsorption free energy and (b) *OOH adsorption free energy calculated from the GPR (Gaussian Process Regression with Regularization) model with DFT (Density Functional Theory) computed values.

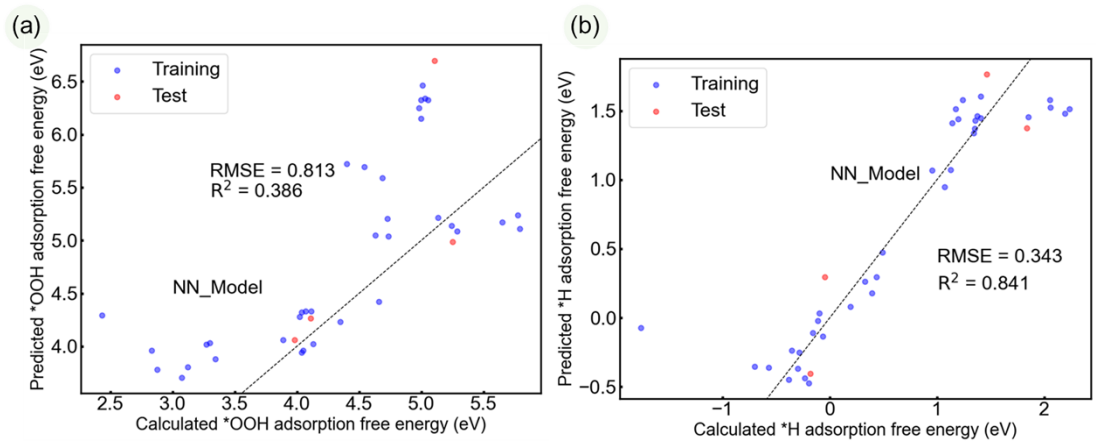

Figure S36. Comparison of (a) *H adsorption free energy and (b) *OOH adsorption free energy calculated from the NN (Neural Network) model with DFT (Density Functional Theory) computed values.

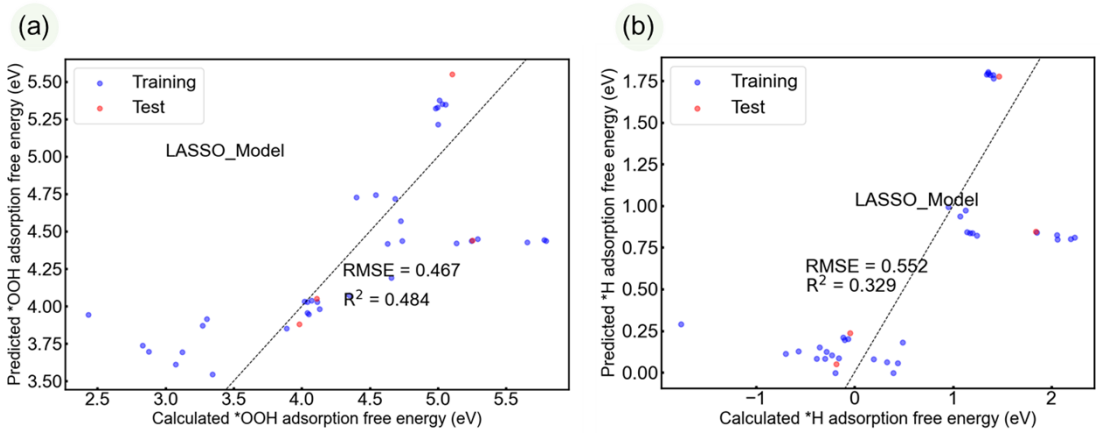

Figure S37. Comparison of (a) *H adsorption free energy and (b) *OOH adsorption free energy calculated from the LASSO model with DFT (Density Functional Theory) computed values.

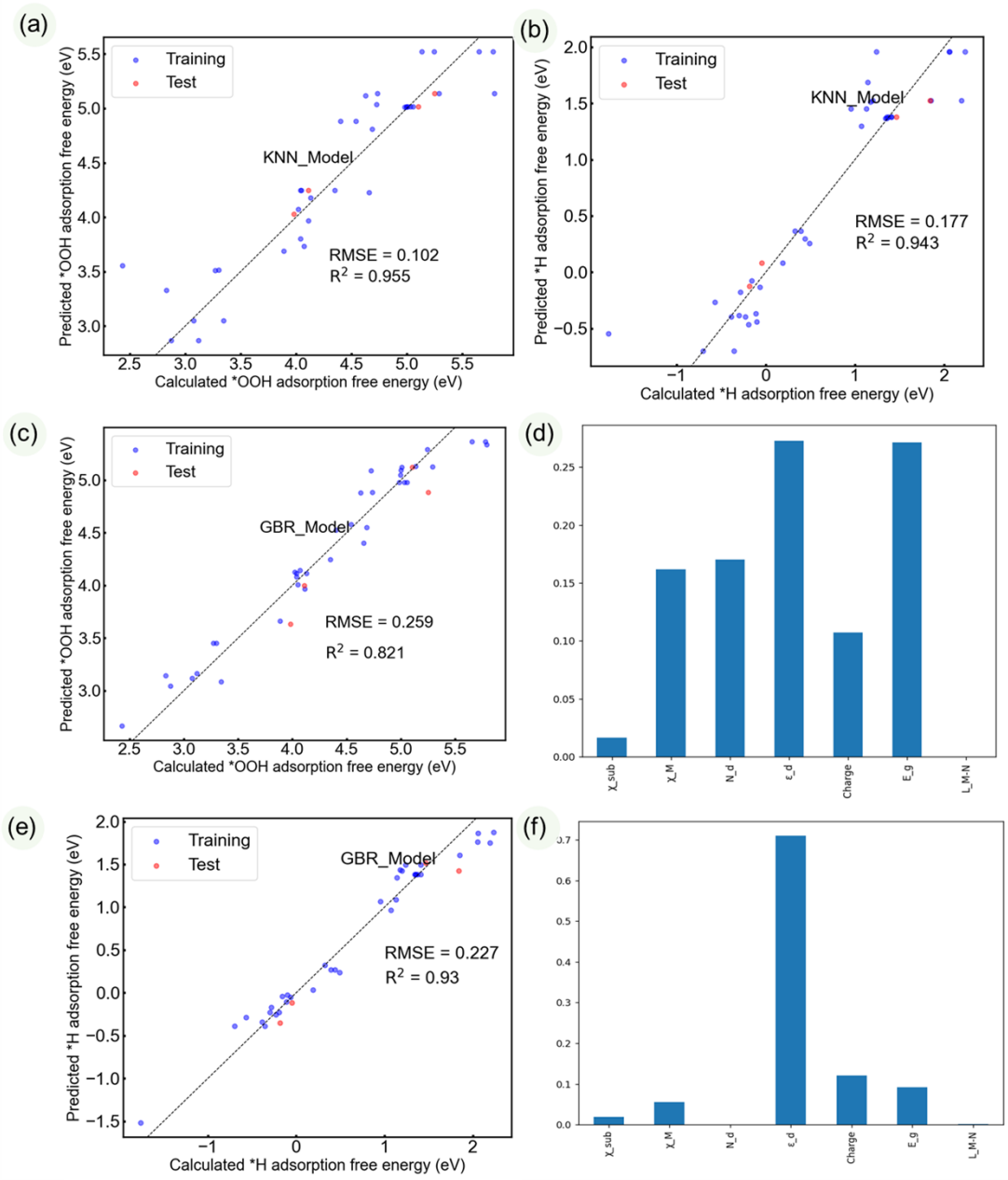

Figure S38. Comparison of (a) *OOH adsorption free energy and (b) *H adsorption free energy calculated from the KNN model with DFT (Density Functional Theory) computed values, removing the M-O/M-H lengths as a descriptor. Comparison of (c) *OOH adsorption free energy and (e) *H adsorption free energy calculated from the GBR model with DFT (Density Functional Theory) computed values and importance analysis of each feature for (d) *OOH adsorption free energy and (f) *H adsorption free energy. removing the M-O/M-H lengths as a descriptor.

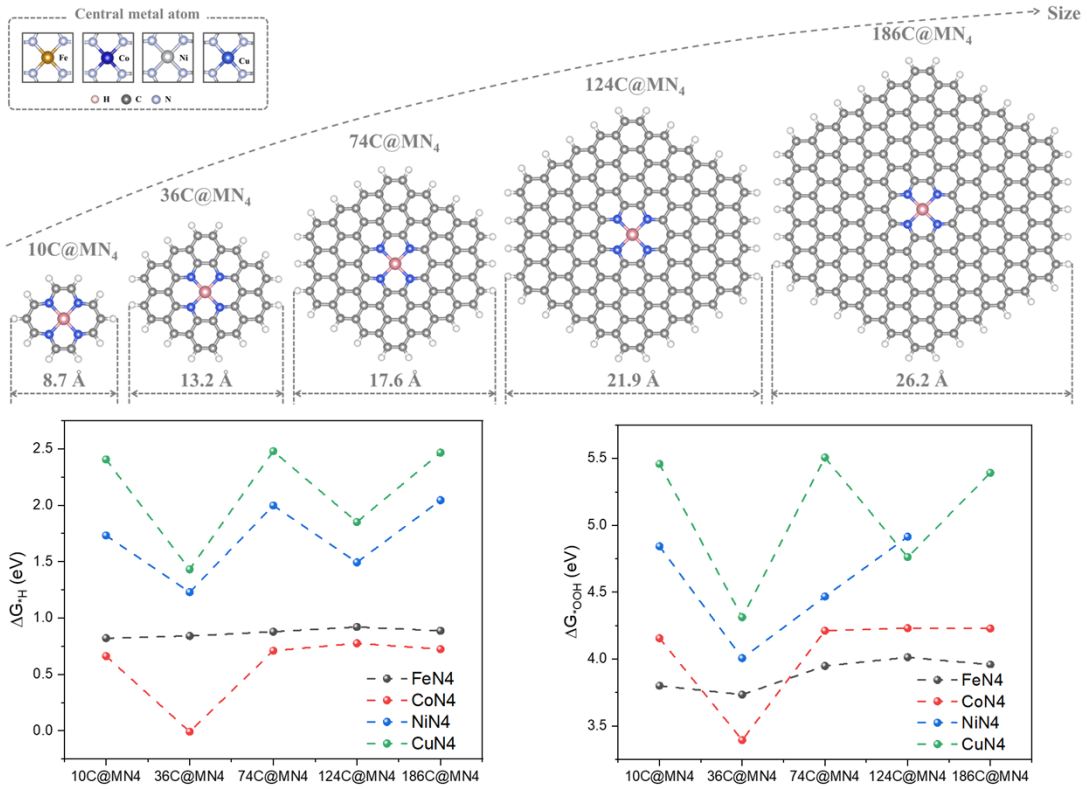

Figure S39. MN_4 configurations of different sizes and their effects on adsorption properties of *H and *OOH.

References:

(1) J. G. Brandenburg, C. Bannwarth, A. Hansen and S. Grimme, *Journal of Chemical Physics*, 2018, 148, 064104.
(2) F. Neese, *Wiley Interdiscip Rev Comput Mol Sci*, 2017, e1327.
(3) F. Neese, *Wiley Interdiscip Rev Comput Mol Sci*, 2022, 12.
(4) F. Neese, F. Wennmohs, U. Becker and C. Riplinger, *Journal of Chemical Physics*, 2020, 152, 224108.